Accepted to J. Chem. Phys. 10.1063/5.0110977

Vibrational energy levels and predissociation lifetimes of the $A^2\Sigma^+$ state of SH/SD radicals by photodissociation spectroscopy

Yuan Qin, Xianfeng Zheng[a], Yu Song[b], Ge Sun[c], and Jingsong Zhang*

Department of Chemistry

University of California at Riverside

Riverside, California 92521

U.S.A.

Abstract

Photo-predissociation of SH and SD radicals in the $A^2\Sigma^+$ state are investigated using the high-*n* Rydberg atom time-of-flight (HRTOF) technique. By measuring the photoproduct translational energy distributions as a function of excitation wavelength, contributions from overlapping $A^2\Sigma^+$ (v') ← $X^2\Pi$ (v'') transitions can be separated, and the H/D + S(^3P_J) photofragment yield (PFY) spectra are obtained across various rovibrational levels (SH v' = 0-7 and SD v' = 0-8) of the $A^2\Sigma^+ \leftarrow X^2\Pi$ bands. The upper $A^2\Sigma^+$ state vibrational levels v' = 5-7 of SH and v' = 3-8 of SD are determined for the first time. The PFY spectra are analyzed with the simulation program *PGOPHER* [Western, *J. Quant. Spectrosc. Radiat. Transfer*, **186**, 221 (2016)], which gives vibrational origins and linewidths of the rovibrational levels of the $A^2\Sigma^+$ state. The linewidths (≥ 1.5 cm^{-1}) of the SH $A^2\Sigma^+$ v' = 3-7 and SD $A^2\Sigma^+$ v' = 2-8 states are characterized for the first time in this work, demonstrating that these levels undergo rapid predissociation with lifetimes on the order of picosecond. The lifetimes of the SD $A^2\Sigma^+$ v' = 0, N' = 1 and 2 levels are determined to be

247±50 ns and 176±60 ns by pump-probe delay measurements, respectively. The experimentally measured lifetimes are in a reasonable agreement with the theoretical predictions.

a. Permanent address: Department of Physics, Anhui Normal University, Wuhu, Anhui 241000, P. R. China.

b. Permanent address: Beijing Academy of Quantum Information Sciences, Beijing, 100193, P. R. China.

c. Current address: Dalian Institute of Chemical Physics, Chinese Academy of Sciences, Dalian, Liaoning 116023, P. R. China.

* Corresponding author. E-mail: jingsong.zhang@ucr.edu. Fax: 1-951-827-4713. Also at the Air Pollution Research Center, University of California, Riverside, CA 92521, USA.

I. Introduction

The SH radical is an important intermediate in atmospheric sulfur chemistry and in fossil fuel combustion processes producing sulfur-containing pollutants. SH is also of interest in astrochemistry and has been detected in various astronomical environments.

The low-lying electronic states of the SH/SD radicals have been well studied with experiments and theories. Figure 1 presents the potential energy curves (PECs) of the SH/SD systems. The ground electronic state, $X^2\Pi$, correlates to the ground state H/D(^{2}S) + S(^{3}P$_J$) products. The first electronically excited $A^2\Sigma^+$ state correlates asymptotically to the excited state products H/D(^{2}S) + S(^{1}D), and it is crossed by three repulsive states, $^4\Sigma^-$, $^2\Sigma^-$, and $^4\Pi$, which correlate with the ground state products H/D(^{2}S) + S(^{3}P$_J$). As a primary detection method, the spectroscopy of the SH and SD $A^2\Sigma^+$–$X^2\Pi$ band systems has been extensively investigated. Lewis and White[1] measured the first absorption spectrum of SH and detected the $A^2\Sigma^+$–$X^2\Pi$ (0,0) band. Ramsay[2] and later Johns and Ramsay[3] measured the UV absorption spectra of the A–X (0,0), (1,0) and (2,0) bands of SH and SD from flash photolysis of H_2S and D_2S. The emission spectra for the SH (0,0) and SD (0,0) and (1,0) bands were measured by Pathak and Palmer.[4] In these observations for SH, the A–X (0,0) band showed sharp rotational structures while the (1,0) and (2,0) bands were diffuse, indicating the onset of rapid predissociation of the $A^2\Sigma^+$ state. Schnieder et al.[5] obtained the empirical term values of the SH $A^2\Sigma^+$ v' = 0-4 produced from photodissociation of H_2S at 121.6 nm. More recently, the spectrum of the SH A–X (0,0) band was investigated by Fast and Meek[6] using frequency comb referenced spectroscopy, which provided improved measurements with an uncertainty of less than 1 MHz. Associated with the available experimental data, theoretical calculations were carried out to predict the A–X line positions by Zahnle et al.[7] for SH (v' = 0-2, v'' = 0-4) and later by Gorman et al.[8] for SH (up to v' = 4) and SD (up to v' = 6).

The predissociation of the $A^2\Sigma^+$ state of SH and SD is attributed to its curve crossings and spin-orbit interactions with the three repulsive $^4\Sigma^-$, $^2\Sigma^-$, and $^4\Pi$ states, which significantly affect the lifetime of the $A^2\Sigma^+$ state. The radiative lifetime of the SH $A^2\Sigma^+$ $v' = 0$, $N' = 0$-10 states were experimentally determined to be 820±240 ns (730±180 ns for SD),[9] while the laser-induced fluorescence (LIF) studies gave predissociative lifetimes of 3±2 ns[9] and 3.2±0.3 ns[10] for SH $A^2\Sigma^+$ $v' = 0$, $N' = 0$. A lower limit of the lifetime of 0.17 ns for SH $A^2\Sigma^+$ ($v' = 0$, $N' = 3$) was determined from LIF spectra using the Hanle effect by Loge and Tiee,[11] which was found later to be altered by power broadening.[12] The SD $v' = 0$, $N' = 0$ level undergoes a slower predissociation, with a lifetime of about 200 ns from the fluorescence measurements.[9, 13, 14] Using cavity ring-down spectroscopy Wheeler et al.[15, 16] measured the linewidths and determined the lifetimes of 5.45-4.61 ps for the SH $v' = 1$, $N' = 0$-8, 35-24 ps for SD $v' = 1$, and 2.31 ps for SD $v' = 2$. Parker and co-workers[17] studied the S(^3P_J) products from predissociation of SH and SD $A^2\Sigma^+$ ($v' = 0$-2) using velocity map imaging, and the dominant S($^3P_2$) products indicated that the predissociation at those levels can be attributed to the spin-orbit coupling with the $^4\Sigma^-$ state. For the higher vibrational levels (SH $v' \geq 2$ and SD $v' \geq 3$), the involvement of the $^2\Sigma^-$ and $^4\Pi$ states should increase, but the lifetimes were not studied experimentally. On the theoretical side, Wheeler et al.[15] employed Fermi Golden Rule calculations to determine the predissociative lifetime of SH $A^2\Sigma^+$ ($v' = 0$-5), by using the experimentally derived analytical potential for the $A^2\Sigma^+$ state and the *ab initio* $^4\Sigma^-$, $^2\Sigma^-$, and $^4\Pi$ potentials and spin-orbit couplings by Manaa.[18] Resende and Ornellas[19] calculated the radiative and predissociative lifetimes for the SH and SD $A^2\Sigma^+$ ($v' = 0$-2) with their *ab initio* potentials and the $^4\Sigma^- - A^2\Sigma^+$ spin-orbit coupling. Later on, Brites et al.[20] extended the lifetime predications to $v' = 0$-6 for SH and $v' = 0$-9 for SD, incorporating the spin-orbit couplings between $A^2\Sigma^+$ and all the three repulsive states from *ab initio* potentials into the Fermi Golden Rule calculations. By taking

the previous theoretical results of potentials and spin-orbit couplings into close coupling methods, Lee and Seon[21] computed the widths and positions of the $A^2\Sigma^+$ (v' = 0-6) ← $X^2\Pi$ (v'' = 0) resonances. More recently, Zhao et al.[22] adopted the multi-reference configuration interaction method plus Davidson correction to calculate the PECs of the low-lying states of SH, and the radiative lifetimes of the $A^2\Sigma^+$ state (v' = 0-3) were evaluated with consideration of scalar relativistic effect, core-valence electron correlation, and spin–orbit coupling effect. These calculations indicated that the lifetime of $A^2\Sigma^+$ state varies with v' and is on the order of several picoseconds for the higher vibrational levels.

The experimental characterization of the $A^2\Sigma^+$ state vibrational energy levels has been somehow hindered by the rapid predissociation, and reliable information for higher vibrational levels is still lacking. The vibrational constants ω_e and $\omega_e x_e$ of SH $A^2\Sigma^+$ have been determined from experimental measurements of lower v' vibrational states, to be 1971 and 93 cm^{-1} (v' = 0-1),[2] 1979.8 and 97.65 cm^{-1} (v' = 0-2),[3] and 1982.9 and 105.92 cm^{-1}(v' = 0-4),[5] respectively, whereas the theoretical studies have predicted different values: 1957.6-2032.25 cm^{-1} for ω_e and 85.18-107.1 cm^{-1} for $\omega_e x_e$.[8, 19-22] For SD, only the vibrational levels v' = 0-2 have been experimentally measured, giving the constants ω_e = 1417.0 cm^{-1} and $\omega_e x_e$ = 48.8 cm^{-1},[3] which are closer to the theoretical results of 1406.0-1420.0 cm^{-1} for ω_e and 43.97-49.50 cm^{-1} for $\omega_e x_e$.[8, 15, 19, 20] The considerable difference between the theoretical predictions and the previous experimental measurements of spectroscopic constants of the SH $A^2\Sigma^+$ state suggests the need for further experimental and theoretical investigations.

In this work, the high-n Rydberg atom time-of-flight (HRTOF) technique is utilized to probe all vibrational levels of the $A^2\Sigma^+$ state (v' = 0-7 for SH and v' = 0-8 for SD). The HRTOF technique permits spectroscopic studies of the highly predissociative levels of the $A^2\Sigma^+$ state, as it

detects the H/D atom products from the predissociation directly. By measuring the H/D + S(^3P_J) product translational energy distributions from photodissociation of SH and SD across the A−X transitions, the photofragment yield (PFY) spectra from specific rovibrational levels of the $A^2\Sigma^+$ state are obtained. From the PFY spectra the predissociation lifetimes and the vibrational origins of the $A^2\Sigma^+$ state are determined. With a much longer lifetime (~200 ns), the dissociation of the SD $A^2\Sigma^+$ $v' = 0$ state is studied using pump-probe measurements of the predissociation products.

II. Experimental

The HRTOF technique was used in this study and the detailed description of the experimental setup has been reported in previous publications.[23-26] A mixture of ~ 6% H_2S (≥ 99.5%, Aldrich) or ~ 9% D_2S (≥ 98%, Cambridge Isotope Laboratories) precursors in Ar (at a total pressure of ~ 1.2 atm) was expanded through a pulsed nozzle. In front of the nozzle the SH or SD molecular beam was generated by photolyzing the precursors with a 193 nm radiation from an ArF excimer laser. The SH/SD radicals produced from the H_2S/D_2S photolysis were subsequently cooled by supersonic expansion and collimated by a skimmer downstream into the high-vacuum main chamber. Crossed with a tunable, linearly polarized UV photodissociation laser radiation (280-333 nm, 5 to 15 mJ/pulse, linewidth ~ 0.3 cm^{-1}) (defined as the photodissociation laser/radiation throughout this work), the SH/SD radicals were photodissociated in the region of intersection. A wavemeter (Burleigh WA-4500) was used to monitor the absolute photodissociation wavelength. The polarization of the photodissociation radiation can be rotated by a Fresnel-Rhomb achromatic λ/2 plate for product angular distribution measurements. The effective rotational temperature of the SH radicals in the beam was estimated to be ~ 45 K (~ 25 K for the SD radicals), based on the relative signal intensities from several initial rotational levels

of the $X^2\Pi$ v'' = 0 ground state. To measure the H-atom photofragment yield (PFY) spectra and photofragment translational energy distributions for specific rovibrational state of SH and SD $A^2\Sigma^+$ (v' = 0-2), the photodissociation laser wavelength was tuned around the resonant excitations of the previously studied SH and SD transitions [$A^2\Sigma^+$ (v' = 0-2, N', J', F_1) ← $X^2\Pi$ (v'' = 0, N'', J'', F_1)].[2, 3] The higher rovibrational levels ($v' \geq 3$) of the SH and SD $A^2\Sigma^+$ state were reached by scanning the photodissociation laser across the vibrational bands, which were initially predicted using the spectroscopic constants.[5, 19, 21] After the photodissociation, the H/D-atom products were pumped by two-color resonant excitation (121.6 nm + 366.2 nm), i.e., from 1^2S to 2^2P state via the Lyman-α transition and then to a metastable high-n Rydberg state (n ~ 30 and with a binding energy of ~ 15 meV). A small portion of the Rydberg H/D atoms drifted with nascent velocities toward a microchannel plate (MCP) detector, and were field ionized in an electric field of ~ 1.5×10^6 V/m at about 2 mm in front of the detector and detected. The effect of the field ionization on the neutral flight time was negligible. The flight length was calibrated to be 37.27 cm by the photodissociation of HBr, with the well-known bond dissociation energy and spin-orbit splitting energy between the Br ($^2P_{3/2}$) and Br ($^2P_{1/2}$) products. The H/D-atom TOF spectra were typically accumulated with ~20-80 k laser firings. The PFY spectra (action spectra) were obtained by integrating the product translational energy distributions derived from the net HRTOF spectra (see more details in the Results section) as a function of the photodissociation wavelength.

III. Results

A. Photofragment yield (PFY) spectra

The observed $A^2\Sigma^+$–$X^2\Pi$ (v',v'') bands include SH (m,0) (m = 0-3), (n,2) (n = 4-6), and (7,3), and SD (m,0) (m = 0-4), (5,1), (n,2) (n = 5-8), (7,3), and (8,3). The H/D-atom TOF spectra

of these bands contained several sharp peaks and a weak broad background. When turning off the 193-nm radiation for radical production, only the weak broad background was present (which was from photolysis of precursors in the beam[23]). The net H-atom signals from the photodissociation of SH were then obtained by removing the broad background with the 193-nm photolysis laser off from the spectra with the 193-nm laser on. When the UV photodissociation laser scanned off the $A^2\Sigma^+$ state resonances, nearly all the sharp peaks vanished, confirming their origin from the $A^2\Sigma^+$ state predissociation. Some minor peaks remained in certain off $A^2\Sigma^+$ state resonance spectra, which were attributed to transitions from the excited vibrational states of $X^2\Pi$ (v" = 2, 3 or 4) to the repulsive $^2\Sigma^-$ state, or from the $X^2\Pi$ (v" = 3, 4, or 5) states to the repulsive wall of the $A^2\Sigma^+$ state.[27] Some $A^2\Sigma^+ \leftarrow X^2\Pi$ transition bands from different initial vibrational states v" have close excitation energies and might accidentally overlap. For instance, the SH (2,1) and (4,2) transitions have nearly the same excitation energy and can be excited by the same laser excitation (Figure 2). Due to the much smaller Franck-Condon factors to the repulsive $^2\Sigma^-$ state from $X^2\Pi$ (v" = 2) in this wavelength region, there was little contribution from the $^2\Sigma^- \leftarrow X^2\Pi$ (v" = 2) transition to the signals of the SH $A^2\Sigma^+$ (v' = 4-6) $\leftarrow X^2\Pi$ (v" = 2) resonances. This was similar in the case of the SD $A^2\Sigma^+$ (v' = 5-8) $\leftarrow X^2\Pi$ (v" = 2, 3) bands. The intensities of the strong peaks in the TOF spectra showed linear dependence on the photodissociation laser power, and their positions and corresponding product translational energies were consistent with the photodissociation photon energy and the SH/SD bond dissociation energy.[23, 24] The above observations unambiguously confirmed that the signals of the intense sharp peaks in the H/D-atom TOF spectra were from predissociation of the SH/SD radical via the $A^2\Sigma^+$ state.

In order to analyze the contributions of predissociation of different vibrational levels of $A^2\Sigma^+$ excited from various initial vibrational states of $X^2\Pi$, the net H/D-atom TOF spectra are

converted to the center-of-mass (CM) product translational energy distributions, $P(E_T)$'s, with the following equation (using SH as the example):[28]

$$E_T = \left(1 + \frac{m_H}{m_S}\right) E_H + \frac{m_H}{m_S} E_{SH} = \frac{1}{2} m_H \left(1 + \frac{m_H}{m_S}\right) \left(\frac{L}{t_H}\right)^2 + \frac{m_H}{m_S} E_{SH} \quad (1)$$

where E_H and E_{SH} are the laboratory translational energy of the H-atom product and the parent SH radical, L is the length of the TOF path, and t_H is the H-atom flight time. The second term ($\frac{m_H}{m_S} E_{SH}$) is due to the parent SH radical motion in the molecular beam, which is perpendicular to the TOF path. This term is estimated to be ~14 cm^{-1} (~29 cm^{-1} for SD), based on the estimated beam velocity of ~560 m/s for the SH/Ar gas mixture. Figure 2 presents the angle-dependent $P(E_T, \theta)$ distributions of photodissociation of the SH radical at the excitation energy of 31622.14 cm^{-1}, which was centered on the $A^2\Sigma^+$ (v' = 2, N' = 2, J' = 2.5, F_1) ← $X^2\Pi$ (v'' = 0, N'' = 1, J'' = 1.5, F_1) transition [$Q_1(1.5)$], with the linear polarization of the photodissociation radiation perpendicular and parallel to the TOF path. Both spectra show strong signals in the E_T region of 4200-5100 and 6700-7600 cm^{-1}, which were the H + S(^3P_J) products from predissociation of the SH radical via the A−X (2,1) and (4,2) transitions, respectively. The minor peak at around 3000 cm^{-1} was due to direct dissociation of SH ($X^2\Pi$, v'' = 4) via the repulsive wall of the $A^2\Sigma^+$ state, leading to the H + S(^{1}D) products. The peaks around 9300-10000 cm^{-1} corresponded to the H + S(^3P_J) products from direct dissociation of SH via the $^2\Sigma^-$ ← $X^2\Pi$ (v'' = 3) transition. The perpendicular $P(E_T, \theta = 90°)$ distributions had stronger signals, indicating anisotropy in the product angular distributions. The CM product translational energy and angular distributions can be described as $P(E_T, \theta) = \frac{1}{4\pi} P(E_T)[1 + \beta(E_T) P_2(cos\theta)]$, in which $P(E_T)$ is the angle-integrated distribution, β is the anisotropy parameter ($-1 \leq \beta \leq 2$), θ is the angle between the electric vector of the linearly polarized photodissociation radiation and the velocity vector of the detected H-atom product (i.e.,

the direction of the TOF axis), and $P_2(cos\theta)$ is the second Legendre polynomial.[29] The energy-dependent anisotropy parameter, $\beta(E_T)$, can be derived from the product translational energy distributions at the parallel ($\theta = 0°, P_{\parallel}(E_T)$) and perpendicular ($\theta = 90°,\ P_{\perp}(E_T)$) polarization, with $\beta(E_T) = 2\times[P_{\parallel}(E_T) - P_{\perp}(E_T)]/[P_{\parallel}(E_T) + 2P_{\perp}(E_T)]$. At the magic angle $\theta_m = 54.7°$, $P_m(E_T)$ is independent of β and is proportional to $P(E_T)$, and it can be derived as $P_m(E_T) = \frac{1}{3}\times[P_{\parallel}(E_T) + 2P_{\perp}(E_T)]$. The $P(E_T, \theta)$ distributions of the H/D + S(^3P_J) products from other SH and SD $A^2\Sigma^+$ (v') ← $X^2\Pi$ (v'') bands are obtained and analyzed similarly.

B. Determination of predissociation lifetimes

The predissociation lifetimes of several vibrational levels of the SH and SD $A^2\Sigma^+$ state are investigated by measuring the linewidths of the rovibrational transitions in the H/D-atom PFY spectra. The PFY spectra were acquired by integrating the signals of the H/D(^2S) + S(^3P_J) product channel in the $P(E_T, \theta)$ distributions across the SH $A^2\Sigma^+$ (v' = 0-7) and SD $A^2\Sigma^+$ (v' = 0-8) absorption bands as a function of the photodissociation wavelength. Figure 3 and 4 show the PFY spectra of the predissociation of SH from several vibrational levels (v' = 3-6) in the $A^2\Sigma^+$ state. The measured PFY spectra are diffuse with peaks ~10 cm^{-1} wide, and the nearby rovibrational transitions overlap due to the rapid predissociation of SH in the $A^2\Sigma^+$ state. The molecular spectrum simulation program *PGOPHER*[30] is used to fit the PFY spectra and determine the linewidths of rovibrational states of each $A^2\Sigma^+$ (v') ← $X^2\Pi$ (v'') transition band. The simulation of absorption spectrum of a linear molecule with *PGOPHER* is initiated by providing the quantum numbers and spectroscopic parameters such as rotational constants and vibrational origins for the lower and upper states. For the PFY data obtained at a single polarization (perpendicular or parallel), the

fitted intensity is weighted by an angular factor of $(1-\frac{1}{2}\beta)$ and $(1+\beta)$ for the perpendicular and parallel polarizations, respectively. The anisotropy parameter β is simulated across the frequency using a program *Betaofnu*,[31] which can calculate the β value of the photofragments from photodissociation as a function of excitation energy, dissociation lifetime, rotational level, and rotational constant. The β values of the various rovibrational transitions of the SH A−X band are calculated similar to those of OH A−X.[26] Note that the angular factor only affects the relative intensity of the peaks but not their positions. As the peaks in most PFY spectra are diffuse and only partially rotationally resolved, the *PGOPHER* spectroscopy fitting is not sensitive to the rotational constants. Therefore, the rotational constants along with other spectroscopic constants are taken from *NIST WebBook of Chemistry*,[32] except that the vibrational band origin is adjusted and determined from the fitting with the experimental data. The *PGOPHER* fittings for the PFY spectra of the predissociation of SH $A^2\Sigma^+$ v' = 3-6 are also presented in Figure 3 and 4 (v' = 7 not shown here; see Supplementary Material).

The experimental lineshapes in the measured PFY spectra can be represented using Voigt line profiles in the *PGOPHER* fitting, with contributions of the photodissociation laser linewidth [Gaussian function with a full width at half maximum (FWHM) of ~ 0.3 cm^{-1}] and a Lorentzian component related to the natural lifetime of the predissociative state. The Doppler broadening is estimated to be ~ 0.03 cm^{-1} (based on the ~ 45 K SH molecular beam temperature) and can be neglected. In each PFY spectrum, the rotational lines to the final $A^2\Sigma^+$ v', N' = 0-3 levels dominate, and they also overlap. Thus the lifetimes determined from the linewidth are the average for these rotational levels. The experimental predissociation lifetimes of SH $A^2\Sigma^+$ v' = 3-7 determined from the fitted Voigt linewidth and its Lorentzian component w_L in the SH spectra are listed in Table I,

together with comparisons with the previous experimental determinations and theoretical calculations.

The SH (0,0), (1,0) and (2,0) and SD (0,0) and (1,0) PFY spectra reproduced the SH/SD $A^2\Sigma^+$ (v' = 0-2) ← $X^2\Pi$ (v'' = 0) absorption lines in the literature.[2, 3] However, the lifetime of SH $A^2\Sigma^+$ v' = 0 is ~3 ns,[9, 10, 19] it could not be measured from the SH (0,0) band using the PFY spectrum linewidth (limited by the ~0.3 cm^{-1} laser bandwidth in this work) or the pump-probe method (limited by the ~10 ns laser pulse time resolution). This is also the case for the SD $A^2\Sigma^+$ v' = 1 state via the SD (1,0) band, whose lifetime is about 35~47 ps.[15, 20] The linewidth measurements of the SH (1,0) and (2,0) bands were hindered by laser power broadening[33] (due to their more favorable transition probabilities and Franck-Condon factors), and thus are not included in this study either. For the SH (1,0) band [as well as the SH (0,0) and SD (1,0) bands], the pumping rate used in this work was much higher than the predissociation rate, and the excitation could be saturated near the peak of the resonances; the linewidth was thus affected by the power broadening, and the observed lineshapes were predominantly Gaussian shape, indicating the limitation by the laser linewidth and power broadening (see Supplementary Material). When the predissociation rate is larger than the laser pumping rate, the population of the upper predissociative level depletes quickly, leaving the upper-level population always smaller than the lower level. For SH (2,0), the predissociation rate was slightly larger than the laser pumping rate, the depletion of the lower-level population upon excitation was greater on the peak of resonance than on the wings, leading to a reduced absorption near the resonance and a power-broadened Voigt lineshape due to depletion ("depletion power broadening") (see Supplementary Material).[33] For other higher v' bands, such as SH (3,0) and (5,2) and SD (3,0), (6,2), and (8,2), etc., the transition probability and Franck Condon factor are much smaller (because they are more off-diagonal), and the predissociation is also much

faster. The predissociation rate was thus much larger than the laser pumping rate in this work, the depletion of the lower-level population upon excitation was essentially uniform across the resonance, and thus the depletion power broadening was minimal. Consequently, for the higher vibrational states such as SH ($v' \geq 3$) and SD ($v' \geq 2$), the contributions of the depletion power broadening to the linewidths in the PFY spectra were negligible due to the much smaller transition probabilities and the much broader predissociative linewidths, and the Voigt lineshape can be used reliably to extract the lifetimes.

Similar to SH, the SD PFY spectra for the vibrational levels (v' = 2-8) in the $A^2\Sigma^+$ state were constructed from integrating the D-atom TOF spectra across the A−X absorption bands, as shown in Figure 5-9. The *PGOPHER* fittings for the PFY spectra of the predissociation of SD $A^2\Sigma^+$ v' = 2-8 are also shown in Figure 5-9. The measured lifetimes of the SD $A^2\Sigma^+$ v' = 2-8 states from the Voigt lineshape and its Lorentzian component in the fitted PFY spectra are presented in Table II. The measured lifetimes for SH v' = 3-7 and SD v' = 2-8 levels are on the order of picosecond, which are much smaller than their radiative lifetimes ($\tau_{radiative}$ = 820±240 ns for SH v' = 0, $\tau_{radiative}$ = 730±180 ns for SD v' = 0).[9] This fact indicates that predissociation dominates the relaxation processes, and the measured lifetime is approximately equal to the predissociation lifetime for these states. The determined lifetimes show oscillation with respect to the v' state, which is related to the specific predissociation dynamics at each vibrational level.

As the predissociation of SD ($A^2\Sigma^+$ v' = 0) state has a slower rate, the radiative relaxation cannot be ignored when determining the lifetime. The lifetime of SD $A^2\Sigma^+$ (v' = 0) is studied using the pump-probe measurements. Figure 10 (a) presents the integrated $D(^2S) + S(^3P_2)$ product signals of the HRTOF spectra at different photodissociation pump and D-atom probe delay time after the SD radical was excited to the $A^2\Sigma^+$ (v' = 0, N' = 1, J' = 1.5, F_1) state via the $Q_1(1.5)$ transition. The

rise of the signals in the pump-probe delay time region of 0-200 ns indicated formation of the D atom from the predissociation of the SD radical, and the decay of the signals after the peak at ~200 ns was due to the D atom flight out of the interaction region of the photodissociation and probe laser beams. The time profile of the D-atom signals, $S_D(t)$, can be described by the following equation:

$$S_D(t) = N[\exp(-k_2\, t) - \exp(-k_D\, t)] \quad (2)$$

where k_D is the total decay rate constant of the SD $A^2\Sigma^+$ state (including radiative relaxation and predissociation), and k_2 accounts for the decay of the D-atom signals during the detection (such as the D atoms flying out of the intersection region).[34] The fitting of the delay time profile using the above equation (solid line) in Figure 10 (a) reveals a decay rate constant of k_D ~4.05×10^6 s^{-1} for the predissociation of the SD radical. This experimental measurement shows that the natural lifetime of the SD radical in the $A^2\Sigma^+$ $v' = 0$, $N' = 1$ state is 247±50 ns. Likewise, the pump-probe time profile of the D-atom signal from the predissociation of the SD $A^2\Sigma^+$ ($v' = 0$, $N' = 2$, $J' = 2.5$, F_1) state via the $R_1(1.5)$ transition is plotted in Figure 10 (b). The fitting indicates k_D ~5.67×10^6 s^{-1} with a natural lifetime of 176±60 ns for $A^2\Sigma^+$ $v' = 0$, $N' = 2$. As the radiative lifetimes for SD $v' = 0$ from the previous studies are all on the order of several hundred nanoseconds,[9, 14, 19, 35] the upper limit of 910 ns is used to derive the predissociative lifetimes.[15] With the relation between the natural lifetime τ_{nat}, predissociation lifetime τ_{pre}, and radiative lifetime τ_{rad}, $\frac{1}{\tau_{nat}} = \frac{1}{\tau_{rad}} + \frac{1}{\tau_{pre}}$, τ_{pre} is determined to be 339±100 ns for SD $A^2\Sigma^+$ $v' = 0$, $N' = 1$ and 218±100 ns for SD $A^2\Sigma^+$ $v' = 0$, $N' = 2$. As presented in Table II, the SD $v' = 0$ lifetimes in this work agree with the values in the previous studies within the uncertainties.

C. Determination of vibrational origins

The vibrational levels in the SH ground state $X^2\Pi$ (v'' = 0-4) have been well studied.[24, 36-41] The vibrational levels $E(v')$ of the SH $A^2\Sigma^+$ state (v' = 0-7) are derived from the band origins obtained from the spectral fittings in this work, which provides new measurements for the $A^2\Sigma^+$ $v' \geq 4$ levels. While the previous experimental data for the vibrational levels of SD ground state are not higher than v'' = 1,[42] the vibrational origins of the SD $X^2\Pi$ v'' = 2-3 are estimated from the recorded SD (5,1) and (5,2), and (8,2) and (8,3) spectra, resulting a value of 3717.9 cm^{-1} for v'' = 2 and 5502.0 cm^{-1} for v'' = 3. Accordingly, the vibrational levels of the SD $A^2\Sigma^+$ v' = 6-8 levels are obtained from the A−X (6,2), (7,3), and (8,2) bands, respectively. Thus, the SD $A^2\Sigma^+$ v' = 0-8 energy levels are all determined for the first time in this work. The vibrational energy is described by customary polynomials in $(v' + \frac{1}{2})$, relative to the zero-point energy,

$$E(v') = \omega_e(v' + \tfrac{1}{2}) - \omega_e x_e(v' + \tfrac{1}{2})^2 + \omega_e y_e(v' + \tfrac{1}{2})^3 + \cdots \quad (3)$$

where ω_e is the harmonic frequency (in cm^{-1}), and $\omega_e x_e$ and $\omega_e y_e$ are the first and second anharmonicity constants, respectively. On varying the polynomial order, the best fit for the $E(v')$ of the $A^2\Sigma^+$ state as a function of v' is obtained when the order is 5 for SH and 4 for SD. However, the 5-order and 4-order fit is only marginally better than a more compact 3-order fit, and the latter format is thus adopted. The results are listed in Table III (SH) and Table IV (SD) along with the comparisons with the previous investigations.

IV. Discussion

Compared to the conventional absorption spectroscopy, the advantage of measurements using photofragments spectroscopy is demonstrated by the observation of the upper vibrational

levels of $A^2\Sigma^+$ state in SH and SD that are highly predissociative and congested by overlapping transitions. The vibrational levels in the $A^2\Sigma^+$ state with v' = 5-7 of SH and v' = 3-8 of SD are determined for the first time. The acquired PFY spectra are free of overlapping transitions from the other A−X bands originated from different initial vibrational levels in $X^2\Pi$, which have similar excitation energies. For example, the energy difference between the SH $X^2\Pi$ v'' = 1 and $A^2\Sigma^+$ v' = 2 is close to that of the $X^2\Pi$ v'' = 2 and $A^2\Sigma^+$ v' = 4, and both the SH A−X (2,1) and (4,2) bands could be reached with the same excitation energy. The signals of the different A−X bands are well separated in the HRTOF spectra and $P(E_T)$ distributions due to their different photofragment translational energies.

A. Predissociation lifetimes

The radiative lifetimes of the $A^2\Sigma^+$ rovibrational levels are on the order of hundreds of nanoseconds,[9, 14, 35] which are much longer than the predissociation process. Thus, the experimental natural lifetimes are dominated by the predissociation lifetimes. The predissociation times of SH and SD in the $A^2\Sigma^+$ state were determined by using the pump-probe delay and H/D-atom PFY spectrum linewidth measurements, and the results are summarized in Table I and II, along with previous experimental results and theoretical calculations. For the SH $A^2\Sigma^+$–$X^2\Pi$ transitions, our linewidth measurements for v' = 3-5 levels are in good agreement with the earlier calculations by Brites et al.[20] and Lee and Seon,[21] while no previous experimental measurements were available for $v' \geq 2$ for comparisons. Our experimental results and the two theoretical calculations have the same trend in the lifetimes of the v' = 3-5 levels, with the fastest predissociation, i.e., the strongest spin-orbit couplings between $A^2\Sigma^+$ and $^4\Sigma^-$, $^2\Sigma^-$, and $^4\Pi$, occurring at v' = 4. As the v' = 6 level is farther from the crossing points of $A^2\Sigma^+$ and the repulsive

states, the lifetime was predicted to be much longer (11-18 ps) by Brites et al..[20] But Lee and Seon argued that the vibrational wave function of $v' = 6$ accidentally overlaps with the continuum wave function, leading to a broader linewidth of 5.58 cm^{-1} (0.95 ps),[21] which is in agreement with our result of ~1.0 ps. There was no theoretical prediction of the lifetime of SH $A^2\Sigma^+$ $v' = 7$ (it was estimated with limited number of data points to be ~ 1.5 ps in this work). Because of the isotope effects, the vibrational levels of the $A^2\Sigma^+$ state of SD are lower in energy than those in SH. For SD $v' = 0$, it lies far below the crossing point of $A^2\Sigma^+$ and $^4\Sigma^-$, thus the spin-orbit coupling between $A^2\Sigma^+$ and $^4\Sigma^-$ is the dominant factor and tunneling effect would be involved in the predissociation process with a longer lifetime. Our pump-probe delay measurements for SD $A^2\Sigma^+$ $v' = 0$ give a natural lifetime of 247±50 ns for $N' = 1$ and 176±60 ns for $N' = 2$, respectively, which are consistent with the earlier experimental work.[9, 13-15] The predissociation lifetimes of these two levels are determined to be 339±100 ns and 218±100 ns after removing the contribution of the radiative lifetime. As $v' = 2$-8 of SD $A^2\Sigma^+$ lie close to, in between, or above the crossings of the $A^2\Sigma^+$ state and the three repulsive states, they show faster predissociation due to the increased couplings of $A^2\Sigma^+$ with the repulsive states. The data points in the measured SD $A^2\Sigma^+$–$X^2\Pi$ (7,3) spectrum were limited, and the lifetime for SD $A^2\Sigma^+$ $v' = 7$ was determined only approximately to be ~1.5 ps. The lifetimes for the SD $A^2\Sigma^+$ $v' = 2$-8 determined from the linewidth measurements of PFY spectra agree with the predictions by Brites et al.[20], except that the fastest predissociation occurs at $v' = 4$ instead of 5. For SD $A^2\Sigma^+$ $v' = 2$, the lifetime of 1.8±0.3 ps determined from the linewidth in this study is in agreement with the previous experimental measurement by Wheeler et al. near the error limit.[15]

In Table I and II, both the experimental and theoretical lifetimes of SH/SD $A^2\Sigma^+$ state show an oscillatory pattern as a function of v', which can be explained by variation of the magnitude of

the spin-orbit couplings between the $A^2\Sigma^+$ state and the three repulsive states ($^4\Sigma^-$, $^2\Sigma^-$, and $^4\Pi$) at the turning point of each v'. As the calculations suggest that the spin-orbit couplings vary at different internuclear distance and are also of different magnitude for the three repulsive states, the predissociation lifetime of each vibrational level of the $A^2\Sigma^+$ state could be strongly influenced by the relative position of the turning point of the v' level to the crossing points of the $A^2\Sigma^+$ state and the three repulsive states. In other words, for the v' level with an outer turning point closer to the crossings of $A^2\Sigma^+$ state and the three repulsive states, it will undergo faster predissociation. The shortest lifetime of $A^2\Sigma^+$ is observed at SH $v' = 4$ and SD $v' = 4$ level, indicating the strongest overall interactions between the $A^2\Sigma^+$ state and the three repulsive states at these vibrational levels. Overall, for both SH and SD the general agreements between our experimental results and the theoretical lifetimes by Brites et al.[20] and Lee and Seon[21] indicate that the *ab initio* PECs and spin-orbit matrix elements at the crossings between $A^2\Sigma^+$ and $^4\Sigma^-$, $^2\Sigma^-$, and $^4\Pi$ and beyond are accurate, allowing predicting accurate lifetimes for the SH and SD $A^2\Sigma^+$ rovibrational levels. However, there are still some small discrepancies between the experimental lifetimes and theoretical predictions; part of these could be attributed to that the predissociation lifetime depends sensitively on the energy positions of the vibrational levels and that the theoretical energy positions of vibrational levels of the $A^2\Sigma^+$ state may not be as exact.

B. Vibrational energy levels

The previous experimental studies of the $A^2\Sigma^+$ state reported the vibrational levels up to $v' = 4$ for SH and $v' = 2$ for SD, and the agreement between our data and those investigations are excellent. For the SH $v' \geq 5$ levels, theoretical calculations by various groups do not agree with each other and only Lee and Seon's predictions[21] are close to our results, even with significant

difference at v' = 6. This is similar for the derived constants, ω_e, $\omega_e x_e$, and $\omega_e y_e$ of SH. For the case of SD, the calculations up to v' = 6 by Gorman et al. match best with our results, which combined the *ab initio* calculations and empirical refinements.[8] Notwithstanding considerable disagreement at SD v' = 7-8, the resultant ω_e and $\omega_e x_e$ for SD are in close agreement with the previous studies. Apparently, the magnitude of $\omega_e y_e$ indicates that contributions from the second-order anharmonicities are not negligible in the SH/SD system. In addition, the vibrational level v' of the $A^2\Sigma^+$ state can be shifted due to perturbation by the spin-orbit couplings with the repulsive $^4\Sigma^-$, $^2\Sigma^-$, and $^4\Pi$ states. The magnitude of vibrational energy shift in $A^2\Sigma^+$ is governed by these spin-orbit couplings, and thus the magnitude of the shift increases when the v' level gets closer to the crossing points. Depending on the relative position of v' to the crossing points, the energy shifts from the couplings with the three repulsive states might have different signs, i.e., below (above) the crossing points, the shift is negative (positive). As a result, the level between the crossing points might have a small shift, with the counteracting effects from lower and higher crossings. In Lee and Seon's work,[21] the v' = 0 to v' = 3 levels in the SH $A^2\Sigma^+$ state are shifted negatively and the magnitude shows an increasing trend from −0.17 to −4.33 cm^{-1}. For v' = 4, unlike its predissociation rate that is the largest, its energy shift is small (+0.93 cm^{-1}), likely due to the compromise of the two opposing shifts between the crossing points. The v' = 5-6 levels are above the highest crossing point and are shifted positively to higher energies (by +6.27 to +7.47 cm^{-1}).

Jamieson and Cheung performed similar calculations on the shifts of the $A^2\Sigma^+$ vibrational levels in the OH radical and its isotope analogues,[43] which can also help understand the perturbation in the SH/SD systems. Compared to the shifts in SH $A^2\Sigma^+$ by Lee and Seon,[21] the magnitude of the calculated shifts in OH (less than 0.7 cm^{-1}) are much smaller due to the smaller spin-orbit interactions between the $A^2\Sigma^+$ and the three repulsive states. They also found that the $^4\Pi$

induced shifts dominate for levels with energy below −4112 cm^{-1} (relative to the dissociation limit of the OH $A^2\Sigma^+$ state), as the $A^2\Sigma^+$–$^4\Pi$ interaction is the strongest near the outer turning points of these levels. In the higher energy region, the $^4\Sigma^-$ shifts become important since the $A^2\Sigma^+$–$^4\Sigma^-$ interaction gains influence near the turning points of the levels with energies above −4112 cm^{-1}. Among the isotope analogues, the shifts of the $A^2\Sigma^+$ vibrational levels are also close when their energies are accidentally close. When applying these conclusions to the SH/SD system, it is expected that the shift of the $v' = 3$ level of SD is close to that of the $v' = 2$ level of SH, and similarly for the case between the $v' = 7$ level of SD and the $v' = 5$ level of SH. Additionally, predissociation process may also affect rotational constants and fine structure parameters, which were not solved in this study.

V. Conclusions

The $A^2\Sigma^+$–$X^2\Pi$ (v', v'') bands for SH $v' = 0$-7 and SD $v' = 0$-8 are characterized by photodissociation spectroscopy in this study using the HRTOF technique. The predissociation times for SH $v' = 3$-7, as well as SD $v' = 0$ ($N' = 1$ and 2) and $v' = 2$-8, are determined from the H/D atom PFY spectra and pump probe delay profiles. The lifetime measurements indicate predissociation rates for the $A^2\Sigma^+$ state depend markedly on the vibrational level, in agreement with the previous theoretical studies. This work also provides the vibrational state energy for the $A^2\Sigma^+$ state, in which the lower energy levels $v' = 0$-4 for SH and $v' = 0$-2 for SD agree well with previous studies, and the higher levels $v' = 5$-7 for SH and $v' = 3$-8 for SD are determined for the first time. The derived vibrational origins of the $A^2\Sigma^+$ state suggest further theoretical investigation at high vibrational levels is needed.

Supplementary Material

The supplementary material provides additional PFY spectra and *PGOPHER* simulations of vibronic bands that are not included in the main text. The SH (0,0), (1,0), and (2,0) bands and SD (1,0) band are presented to show the photodissociation laser power broadening. The SH (7,3) band is included for the lifetime measurement.

Acknowledgement

We thank Profs. Millard H. Alexander, Paul J. Dagdigian, and Richard Dawes for helpful discussions. This work was supported by the US National Science Foundation (grant number CHE-1566636 and CHE-2155232).

References

[1] M. N. Lewis, and J. U. White, Phys. Rev. **55** (1939) 894.

[2] D. A. Ramsay, J. Chem. Phys. **20** (1952) 1920.

[3] J. Johns, and D. A. Ramsay, Can. J. Phys. **39** (1961) 210.

[4] C. Pathak, and H. Palmer, J. Mol. Spectrosc. **32** (1969) 157.

[5] L. Schnieder *et al.*, J. Chem. Phys. **92** (1990) 7027.

[6] A. Fast, and S. A. Meek, J. Chem. Phys. **154** (2021) 114304.

[7] K. Zahnle *et al.*, Astrophys. J. Lett. **701** (2009) L20.

[8] M. N. Gorman, S. N. Yurchenko, and J. Tennyson, Mon. Not. R. Astron. Soc. **490** (2019) 1652.

[9] R. R. Friedl, W. H. Brune, and J. G. Anderson, J. Chem. Phys. **79** (1983) 4227.

[10] W. Ubachs, J. Ter Meulen, and A. Dymanus, Chem. Phys. Lett. **101** (1983) 1.

[11] G. W. Loge, and J. Tiee, J. Chem. Phys. **89** (1988) 7167.

[12] W. Ubachs, and J. ter Meulen, J. Chem. Phys. **92** (1990) 2121.

[13] M. Kawasaki *et al.*, J. Chem. Phys. **91** (1989) 6758.

[14] J. Tiee, M. Ferris, and F. Wampler, J. Chem. Phys. **79** (1983) 130.

[15] M. D. Wheeler, A. J. Orr-Ewing, and M. N. Ashfold, J. Chem. Phys. **107** (1997) 7591.

[16] M. D. Wheeler *et al.*, Chem. Phys. Lett. **268** (1997) 421.

[17] R. Rose *et al.*, J. Chem. Phys. **130** (2009) 034307.

[18] M. R. Manaa, Int. J. Quantum Chem. **56** (1995) 577.

[19] S. M. Resende, and F. R. Ornellas, J. Chem. Phys. **115** (2001) 2178.

[20] V. Brites, D. Hammoutène, and M. Hochlaf, J. Phys. B: At. Mol. Opt. Phys. **41** (2008) 045101.

[21] S. Y. Lee, and H. S. Seon, Bull. Korean Chem. Soc. **22** (2001) 210.

[22] S.-T. Zhao *et al.*, Chin. Phys. B (2021)

[23] W. Zhou *et al.*, J. Chem. Phys. **123** (2005) 054330.

[24] X. Zheng *et al.*, Phys. Chem. Chem. Phys. **11** (2009) 4761.

[25] G. Sun *et al.*, Chin. J. Chem. Phys. **33** (2020) 129.

[26] G. Sun *et al.*, Mol. Phys. **119** (2021) e1837974.

[27] L. M. Janssen *et al.*, J. Chem. Phys. **126** (2007) 094304.

[28] K. Xu, G. Amaral, and J. Zhang, J. Chem. Phys. **111** (1999) 6271.

[29] R. N. Zare, Mol. Photochem **4** (1972) 1.

[30] C. M. Western, J. Quant. Spectrosc. Radiat. Transf. **186** (2017) 221.

[31] H. Kim *et al.*, J. Chem. Phys. **125** (2006) 133316.

[32] A. Kramida, Yu. Ralchenko, J. Reader, and NIST ASD Team (2021), in *NIST Atomic Spectra Database (ver. 5.9) [Online]*National Institute of Standards and Technology, Gaithersburg, MD, Available: https://physics.nist.gov/asd [accessed 2022 July 17].

[33] J. A. Gray, and R. L. Farrow, J. Chem. Phys. **95** (1991) 7054.

[34] J. Park, R. Bersohn, and I. Oref, J. Chem. Phys. **93** (1990) 5700.

[35] J. Senekowitsch *et al.*, J. Chem. Phys. **83** (1985) 4661.

[36] P. Davies *et al.*, Mol. Phys. **36** (1978) 1005.

[37] R. Winkel Jr, and S. P. Davis, Can. J. Phys. **62** (1984) 1420.

[38] A. Benidar *et al.*, J. Mol. Spectrosc. **147** (1991) 383.

[39] R. Ram *et al.*, J. Mol. Spectrosc. **172** (1995) 34.

[40] B. Ruscic *et al.*, J. Phys. Chem. A **105** (2001) 1.

[41] M. Martin-Drumel *et al.*, Chem. Phys. Lett. **550** (2012) 8.

[42] D. Zeitz *et al.*, Mol. Phys. **54** (1985) 953.

[43] M. Jamieson, and A. S. Cheung, J. Phys. B: At., Mol. Opt. Phys. **38** (2005) 939.

[44] J. K. Park, and H. Sun, Chem. Phys. Lett. **194** (1992) 485.

Figure and Captions

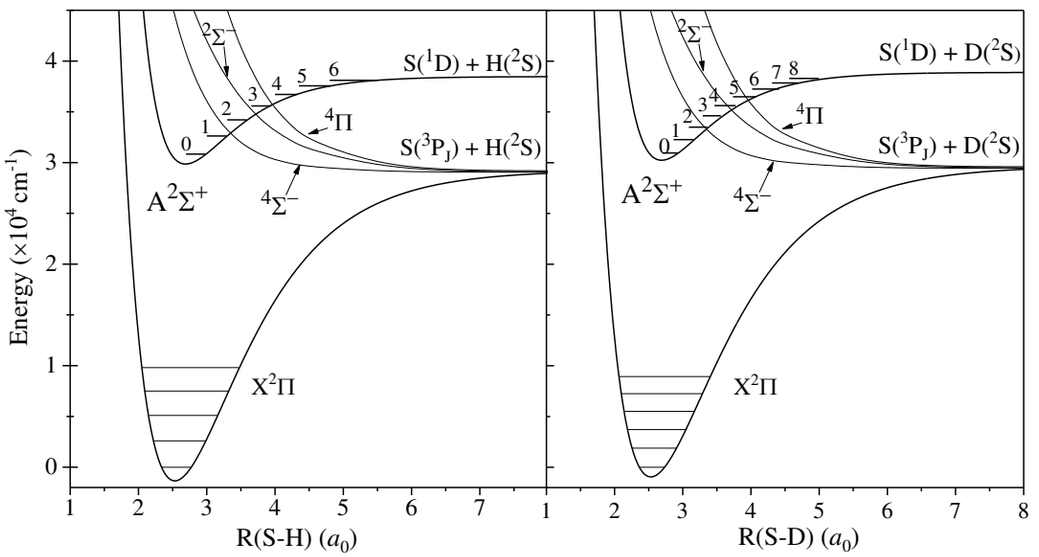

Figure 1 Potential energy curves of the SH and SD electronic states. The vibrational levels of the $A^2\Sigma^+$ state are labelled and shown. The information is from Refs. 18, 19, 44.

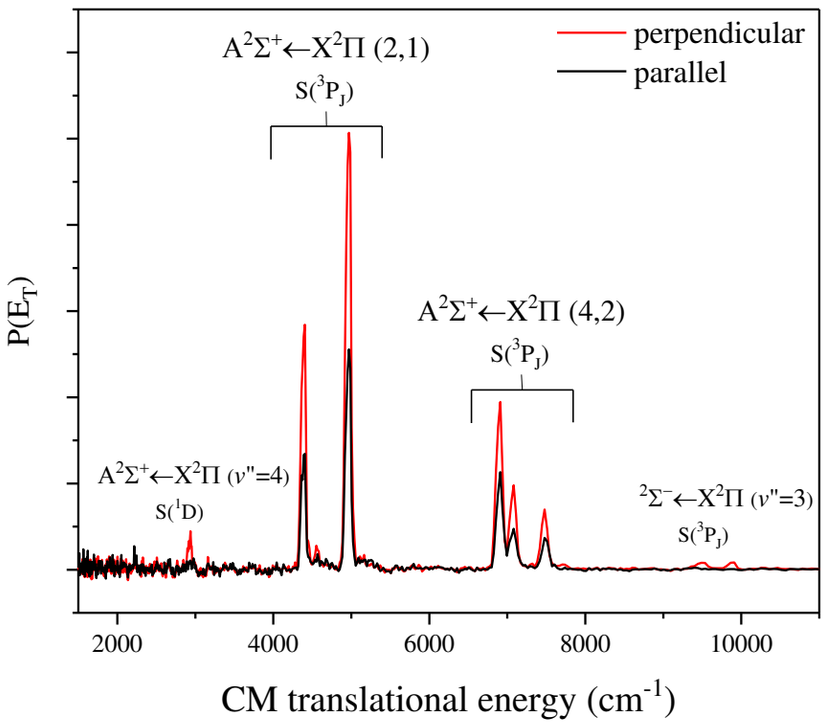

Figure 2 Center-of-mass H + S product translational energy distribution, $P(E_T, \theta)$'s, from photodissociation of SH at 31622.14 cm^{-1}, which is the resonance position of the $A^2\Sigma^+ - X^2\Pi$ (2,1) $Q_1(1.5)$, $^QP_{21}(1.5)$ transition. The $P(E_T)$ distributions are converted from the TOF spectra with the linearly polarized photodissociation radiation perpendicular ($\theta = 90°$) and parallel ($\theta = 0°$) to the TOF path. The products from different pathways are labeled. See text for more details.

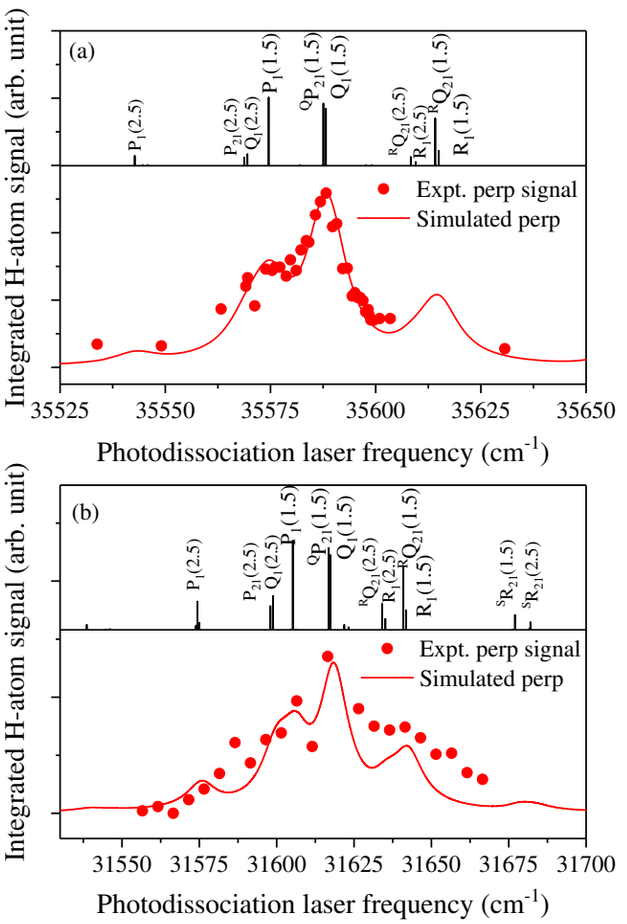

Figure 3 PFY spectra and simulations of the SH $A^2\Sigma^+ - X^2\Pi$ absorption bands (a) (3,0) and (b) (4,2) at perpendicular polarization ($\theta = 90°$) of the photodissociation radiation. The experimental signals (solid circles) were obtained by integrating the H(^{2}S) + S(^3P_J) product peaks from predissociation of SH ($A^2\Sigma^+$, v' = 3 or 4) in the $P(E_T, \theta)$'s. The experimental data were discrete points in frequency as they were obtained from the individual TOF spectra measured at the various laser frequencies. The solid line is the simulation spectrum with T = 30 K in (a), and T = 45 K in (b). The intensity at perpendicular polarization is obtained by weighing the simulated total absorption spectrum (equivalent to PFY at magic angle) from *PGOPHER* with an angular factor of $\left(1 - \frac{1}{2}\beta\right)$, where the anisotropy parameter β is simulated as a function of transition energy using the program *Betaofnu*. With the Gaussian FWHM = 0.3 cm^{-1}, the Lorentzian FWHM is (a) 10.0 cm^{-1} and (b) 11.0 cm^{-1}.

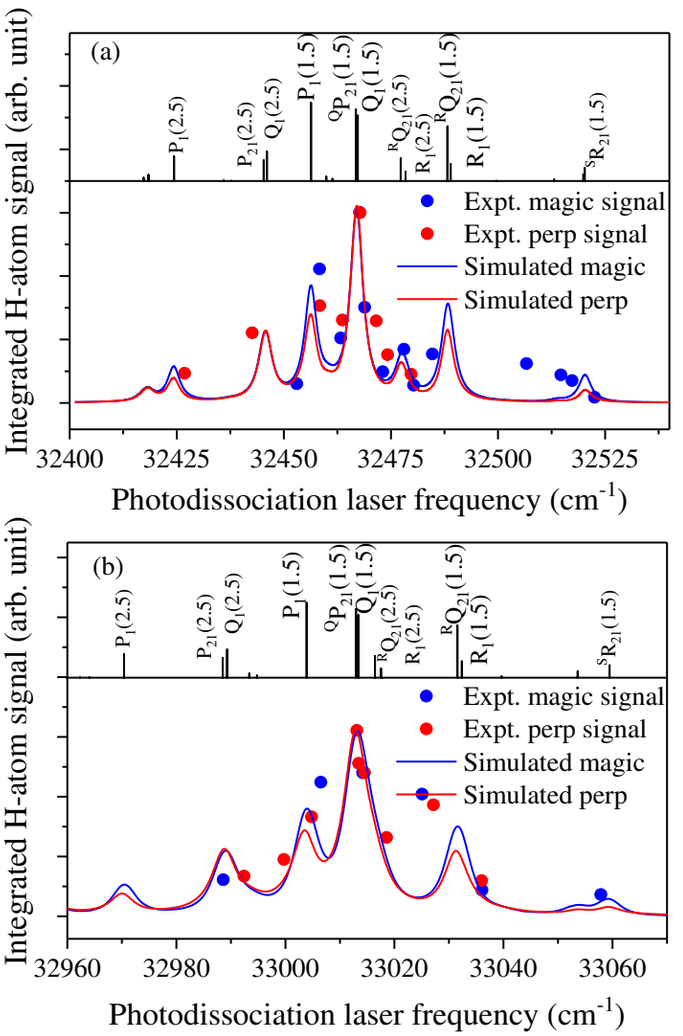

Figure 4 PFY spectra and simulations of the SH $A^2\Sigma^+ - X^2\Pi$ absorption bands (a) (5,2) and (b) (6,2) with the photodissociation radiation polarization at both magic angle ($\theta = 54.7°$) and perpendicular ($\theta = 90°$). In the simulations (T = 45 K), the Gaussian FWHM = 0.3 cm^{-1}, and the Lorentzian FWHM is (a) 3.5 cm^{-1} and (b) 4.4 cm^{-1}.

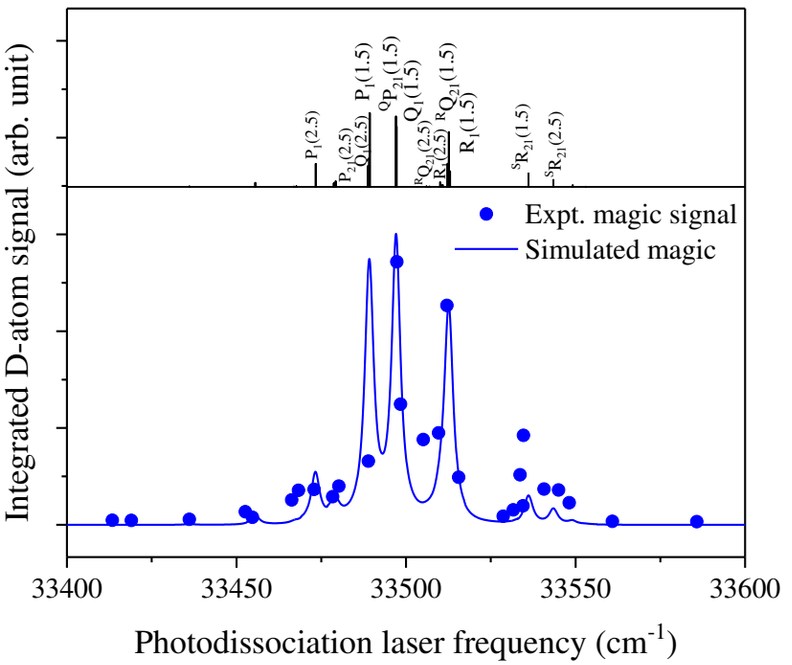

Figure 5 PFY spectra and simulations of the SD $A^2\Sigma^+ - X^2\Pi$ absorption band (2,0) at magic angle ($\theta = 54.7°$). The solid circles represent the integrated D-atom signals from TOF spectra. The solid lines are the simulation results with T = 25 K (same for the following SD spectra). With the Gaussian FWHM = 0.3 cm^{-1}, the Lorentzian FWHM is fitted to be 3.0 cm^{-1}.

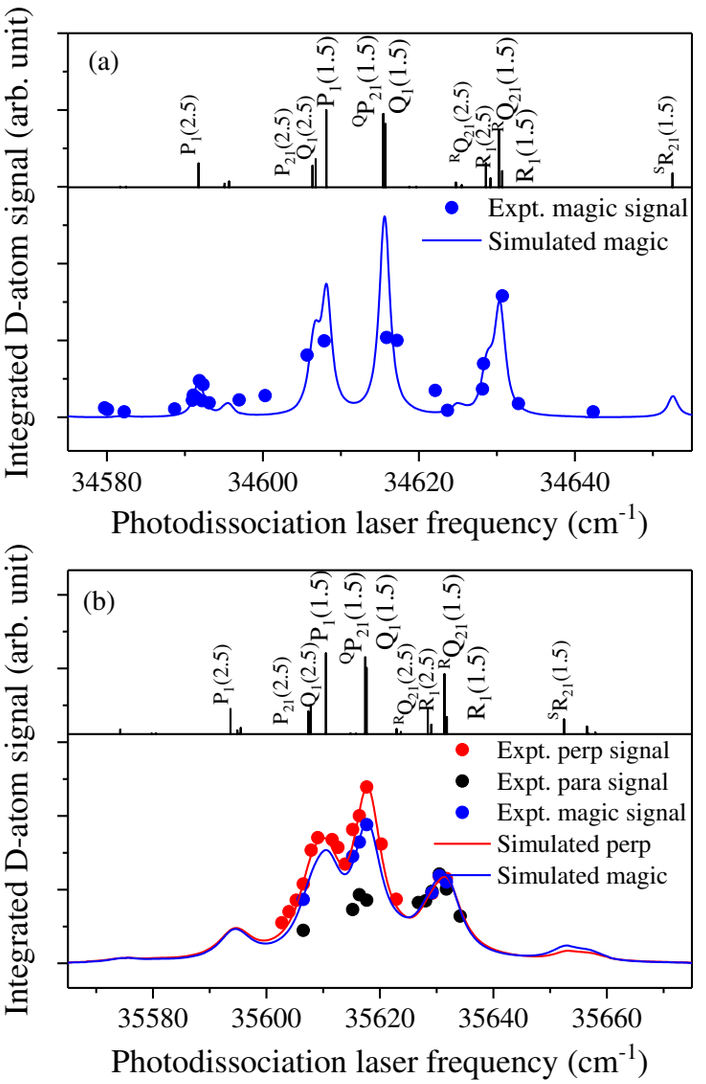

Figure 6 PFY spectra and simulations of the SD $A^2\Sigma^+ - X^2\Pi$ absorption bands (a) (3,0) at magic angle ($\theta = 54.7°$) and (b) (4,0) at different polarizations. With the Gaussian FWHM = 0.3 cm^{-1}, the Lorentzian FWHM is (a) 1.5 cm^{-1} and (b) 5.9 cm^{-1}.

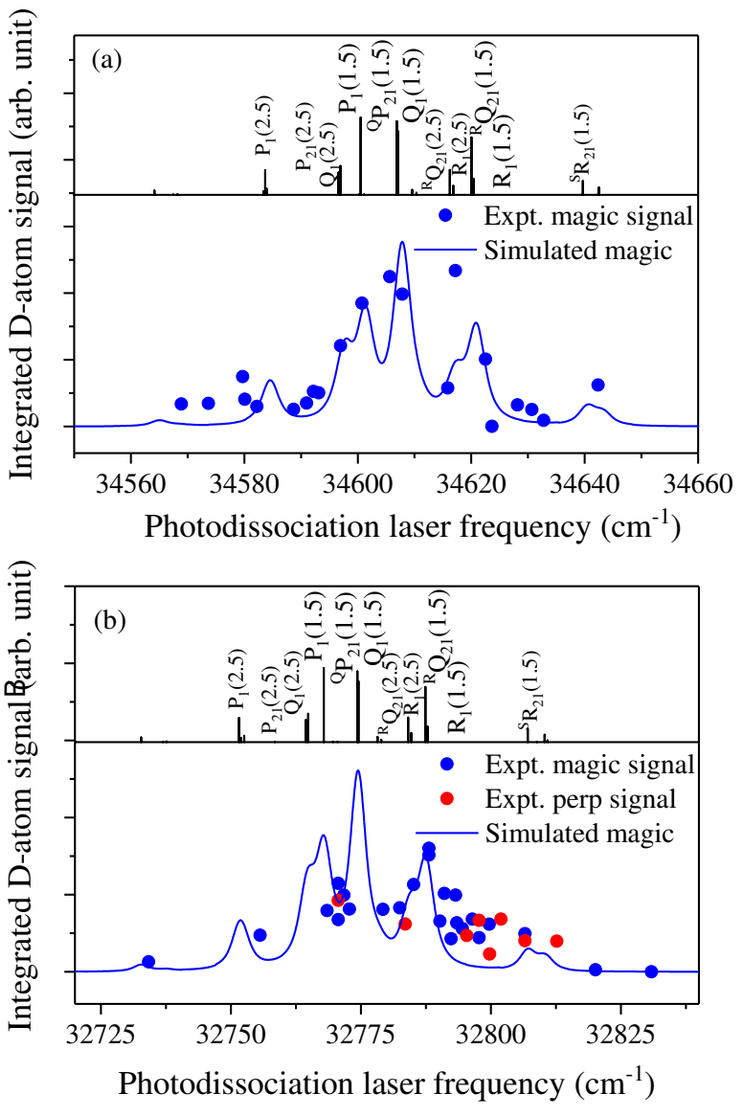

Figure 7 PFY spectra and simulations of the SD $A^2\Sigma^+ - X^2\Pi$ absorption bands (a) (5,1) at magic angle ($\theta = 54.7°$) and (b) (5,2) at magic angle and perpendicular polarization. With the Gaussian FWHM = 0.3 cm^{-1}, the Lorentzian component in both (a) and (b) has FWHM of 3.6 cm^{-1}.

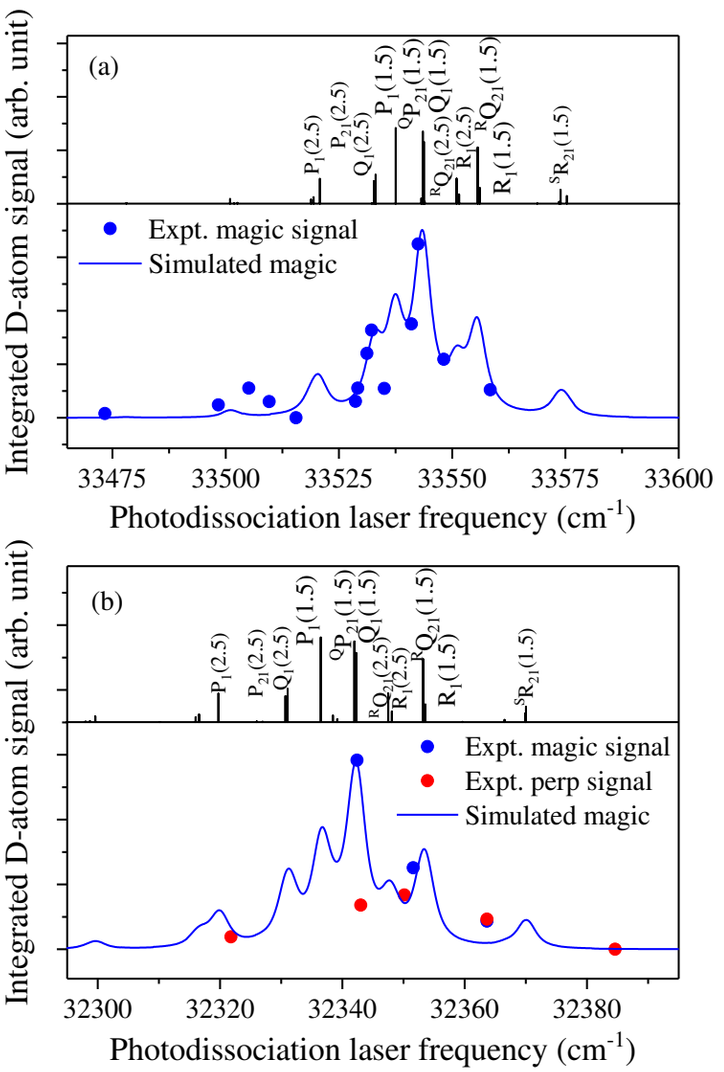

Figure 8 PFY spectra and simulations of the SD $A^2\Sigma^+$–$X^2\Pi$ absorption bands (a) (6,2) at magic angle ($\theta = 54.7°$) and (b) (7,3) at magic angle and perpendicular polarization. With the Gaussian FWHM = 0.3 cm^{-1}, the Lorentzian FWHM is (a) 4.5 cm^{-1} and (b) 3.6 cm^{-1}.

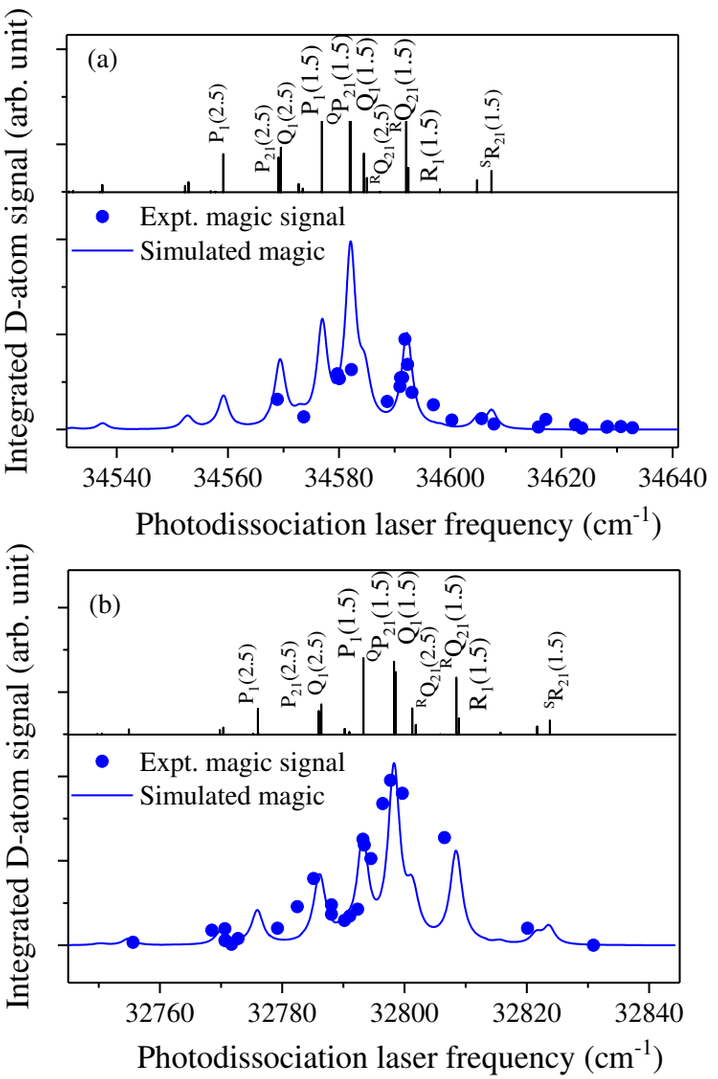

Figure 9 PFY spectra and simulations of the SD $A^2\Sigma^+ - X^2\Pi$ absorption bands (a) (8,2) and (b) (8,3). With the Gaussian FWHM = 0.3 cm^{-1}, the Lorentzian component has FWHM of 2.2 cm^{-1} in both (a) and (b).

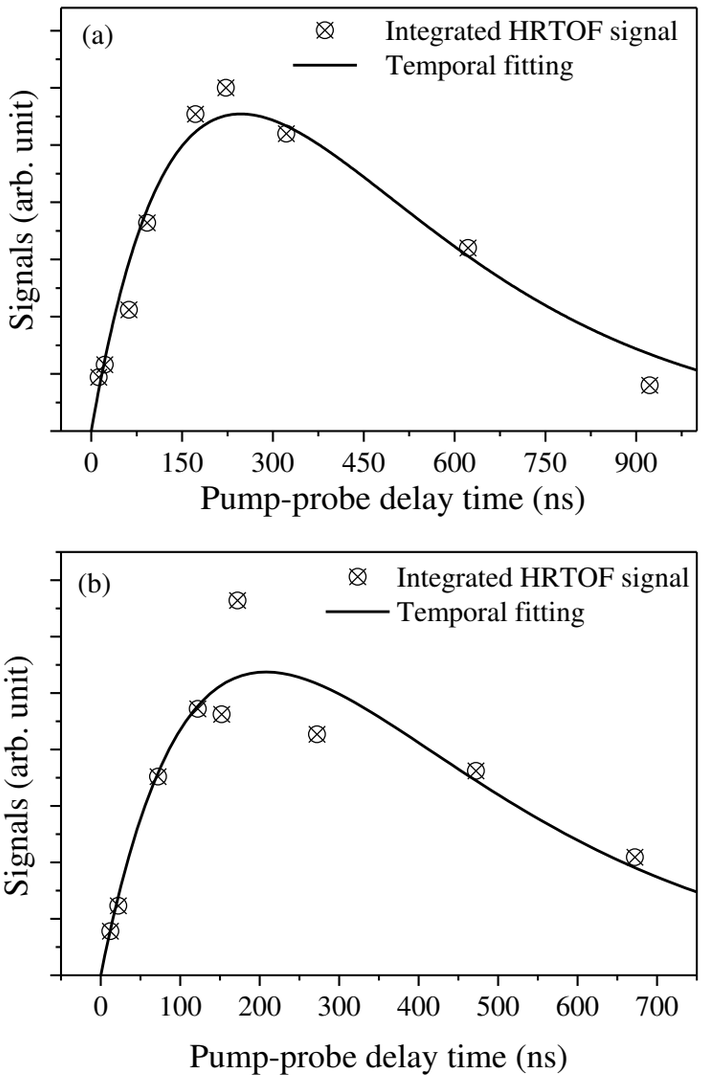

Figure 10 D-atom product temporal profile from predissociation of SD via $A^2\Sigma^+$, $v' = 0$, (a) $N' = 1$, and (b) $N' = 2$. The signals were obtained by integrating the $D(^2S) + S(^3P_2)$ product peaks from the HRTOF spectra of SD via (a) the $Q_1(1.5)$ and (b) $R_1(1.5)$ transition at various photodissociation pump probe delay times. The solid line is the fitting result of the D-atom product time profile. See text for details.

Table I. Lifetimes of the SH $A^2\Sigma^+$ (v' = 0-7).

		Natural						Predissociative		
v'	N'	This work	Expt[a]	Expt[b]	Expt[c]	Expt[d]	Expt[e]	Calc[e]	Calc[f]	Calc[g]
0	0		3±2 ns	3.2±0.3 ns	0.17 ns	3.37±0.13 ns		3.0 ns	6.3 ns	1.10 ns
1	0						5.45 ps	6.1ps	10.6 ps	5.27 ps
2	0							2.3 ps	2.3 ps	2.73 ps
3	0-3	0.53±0.05 ps						0.63 ps	0.95 ps	0.68 ps
4	0-3	0.48±0.14 ps						0.32 ps	0.24 ps	0.62 ps
5	0-3	1.5±0.4 ps						4.0 ps	5.9 ps	2.38 ps
6	0-3	~1.0 ps							0.95 ps	18.25 ps
7	0-3	~1.5 ps								

Note $\frac{1}{\tau_{nat}} = \frac{1}{\tau_{rad}} + \frac{1}{\tau_{pre}}$. As the radiative relaxation of SH $A^2\Sigma^+$ state is much slower (700-800 ns) than the predissociation, its contribution to the natural lifetime can be neglected, i.e., $\tau_{nat} \approx \tau_{pre}$.

[a] Friedl, et al., Ref. 9.
[b] Ubachs, et al., Ref. 10.
[c] Loge and J. Tiee, Ref. 11.
[d] Fast and Meek, Ref. 6.
[e] Wheeler, et al., calculations are all at N'= 0 level, adopted from Ref. 15.
[f] Lee and Seon, at N'= 0 level, Ref. 21.
[g] Brites, et al., at N'= 0 level, Ref. 20.

Table II. Lifetimes of the SD $A^2\Sigma^+$ (v' = 0-8).

		Natural				Predissociative				
v'	N'	This work	Expt[a]	Expt[b]	Expt[c]	This work	Expt[a]	Expt[d]	Calc[d]	Calc[e]
0	0			198±7 ns				247±10 ns[*]	263.2 ns	43.65 ns
	1	247±50 ns	194±20 ns (N'= 0-10)	~195 ns		339±100 ns	260±100 ns (N'= 0-10)		256.9 ns	
	2	176±60 ns		~188.5 ns		218±100 ns		230±5 ns[*]	243.2 ns	
	3				189 ns					
1	0							35 ps	84 ps	46.63 ps
2	0-3	1.8±0.3 ps				1.8±0.3 ps		2.31 ps (N'≈ 0-10)	2.3 ps[†]	2.27 ps
3	0-3	3.5±0.9 ps				3.5±0.9 ps				7.02 ps
4	0-3	0.9±0.2 ps				0.9±0.2 ps				0.91 ps
5	0-3	1.5±0.3 ps				1.5±0.3 ps				0.47 ps
6	0-3	1.2±0.2 ps				1.2±0.2 ps				1.69 ps
7	0-3	~1.5 ps				~1.5 ps				1.03 ps
8	0-3	2.4±0.4 ps				2.4±0.4 ps				2.33 ps

This work: assume τ_{rad}(SD, v'= 0)= 910 ns.
[a] Friedl, et al., with τ_{rad}(SD, v'= 0)= 730±180 ns, Ref. 9.
[b] Kawasaki, et al., Ref. 13.
[c] Tiee et al., Ref. 14.
[d] Wheeler, et al., [*]taken from Ref. 13 with τ_{rad}(SD, v'= 0)= 910 ns; [†]at N'= 0 level, Ref. 15.
[e] Brites, et al., at N'= 0 level, Ref. 20.

Table III. Vibrational levels relative to $v' = 0$ and constants of the SH $A^2\Sigma^+$ ($v' = 0$-7). Unit: cm^{-1}.

v'	This work	Expt[a]	Expt[b]	Calc[c] (perturbed)	Calc[c] (unperturbed)	Calc[d]	Calc[e]	Calc[f]
0	0	0	0	0.0	0	0	0	0
1	1784.42±0.4	1784.5±0.1	1784.5±1.0	1783.56	1784.48	1768.64	1787.24	1784.52
2	3374.01±0.3	3373.7±0.3	3373.7±1.0	3368.88	3369.89	3315.25	3404.12	3373.94
3	4742.19±0.8		4742.8±5.0	4745.23	4749.39	4612.38	4850.64	4755.53
4	5871.88±2		5880.1±10.0	5913.23	5912.13	5622.26	6126.8	5914.32
5	6724.10±0.7			6847.40	6840.96	6305.64	7232.6	
6	7270.91±1.2			7513.93	7506.29		8168.04	
7	~7540.69							
ω_e	1967.5	1979.8	1982.9	1951.2*	1955.6*	1973.8	1957.6	1965.7*
$\omega_e x_e$	83.05	97.65	105.92	82.72*	83.81*	99.67	85.18	86.92*
$\omega_e y_e$	−3.76	⋯	⋯	−2.62*	−2.58*	−1.14	⋯	−2.31*
$\omega_e z_e$	⋯	⋯	⋯	⋯	⋯	−0.43	⋯	⋯

* The constants are obtained from a 3rd-order polynomial fitting with the levels from references.
[a] Johns and Ramsay, Ref. 3.
[b] Schnieder, et al., Ref. 5.
[c] Lee and Seon, Ref. 21. The unperturbed values are without the couplings of the $A^2\Sigma^+$ state with the three repulsive states. The perturbed values inlcude these couplings.
[d] Resende and Ornellas, Ref. 19.
[e] Brites, et al., levels are derived from the constants, Ref. 20.
[f] Gorman, et al., Ref. 8.

Table IV. Vibrational levels relative to $v' = 0$ and constants of the SD $A^2\Sigma^+$ ($v' = 0$-8). Unit: cm^{-1}.

v'	This work	Expt[a]	Calc[b]	Calc[c]	Calc[d]	Calc[e]
0	0	0	0	0	0	0
1	1319.18±0.1	1319.30±0.05	1319.03	1313.0	1313.0	1319.28
2	2540.23±0.3	2540.9±0.2	2541.11	2515.6	2515.6	2540.54
3	3659.85±0.3		3671.34	3600.1	3600.1	3659.85
4	4662.23±0.4		4699.52	4556.2	4744.6	4672.33
5	5536.88±2		5630.75	5370.1	5710.9	5572.38
6	6306.33±0.3		6462.48		6589.26	6353.56
7	~6889.38		7197.26		7379.68	
8	7345.95±0.8		7832.58		8082.16	
ω_e	1400.83	1417.0	1420.0	1416.2	1406.0	1410.6*
$\omega_e x_e$	39.67	48.85	48.95	49.50	43.97	44.56*
$\omega_e y_e$	−1.62	…	…	…	…	−0.87*

* The constants are obtained from a 3rd-order polynomial fitting with the levels from references.
[a] Johns and Ramsay, Ref. 3.
[b] Wheeler, et al., adopted from Ref. 15.
[c] Resende and Ornellas, Ref. 19.
[d] Brites, et al., Ref. 20.
[e] Gorman, et al., Ref. 8.

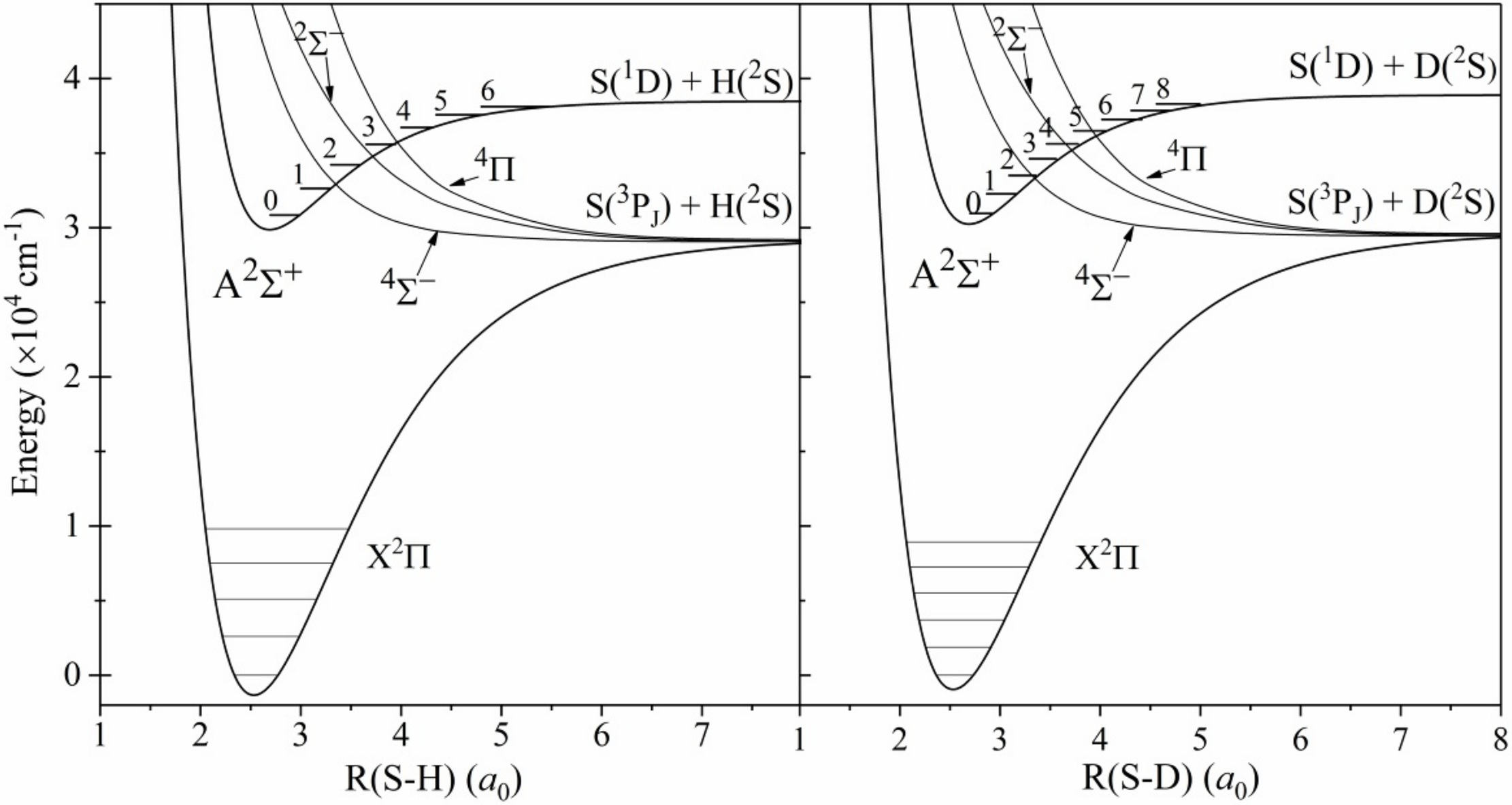
Energy (×10^4 cm^-1)
R(S-H) (a0)
R(S-D) (a0)
S(1D) + H(2S)
S(3PJ) + H(2S)
S(1D) + D(2S)
S(3PJ) + D(2S)
A2Σ+
X2Π
4Σ−
4Π
2Σ−
0
1
2
3
4
5
6
7
8

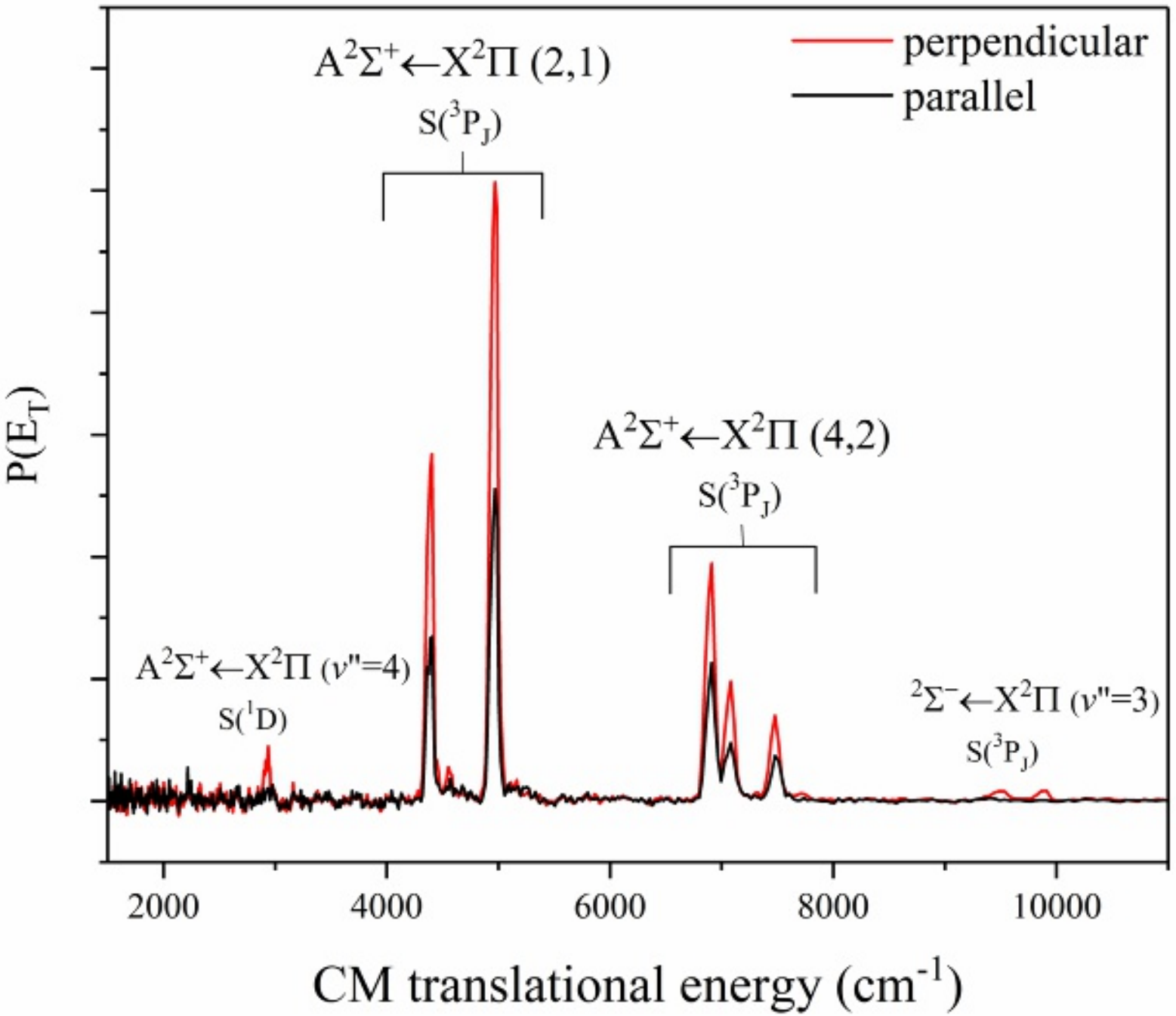
perpendicular
parallel
$A^2\Sigma^+ \leftarrow X^2\Pi$ (2,1)
$S(^3P_J)$
$A^2\Sigma^+ \leftarrow X^2\Pi$ (4,2)
$S(^3P_J)$
$A^2\Sigma^+ \leftarrow X^2\Pi$ (v''=4)
$S(^1D)$
$^2\Sigma^- \leftarrow X^2\Pi$ (v''=3)
$S(^3P_J)$
$P(E_T)$
2000
4000
6000
8000
10000
CM translational energy (cm^{-1})

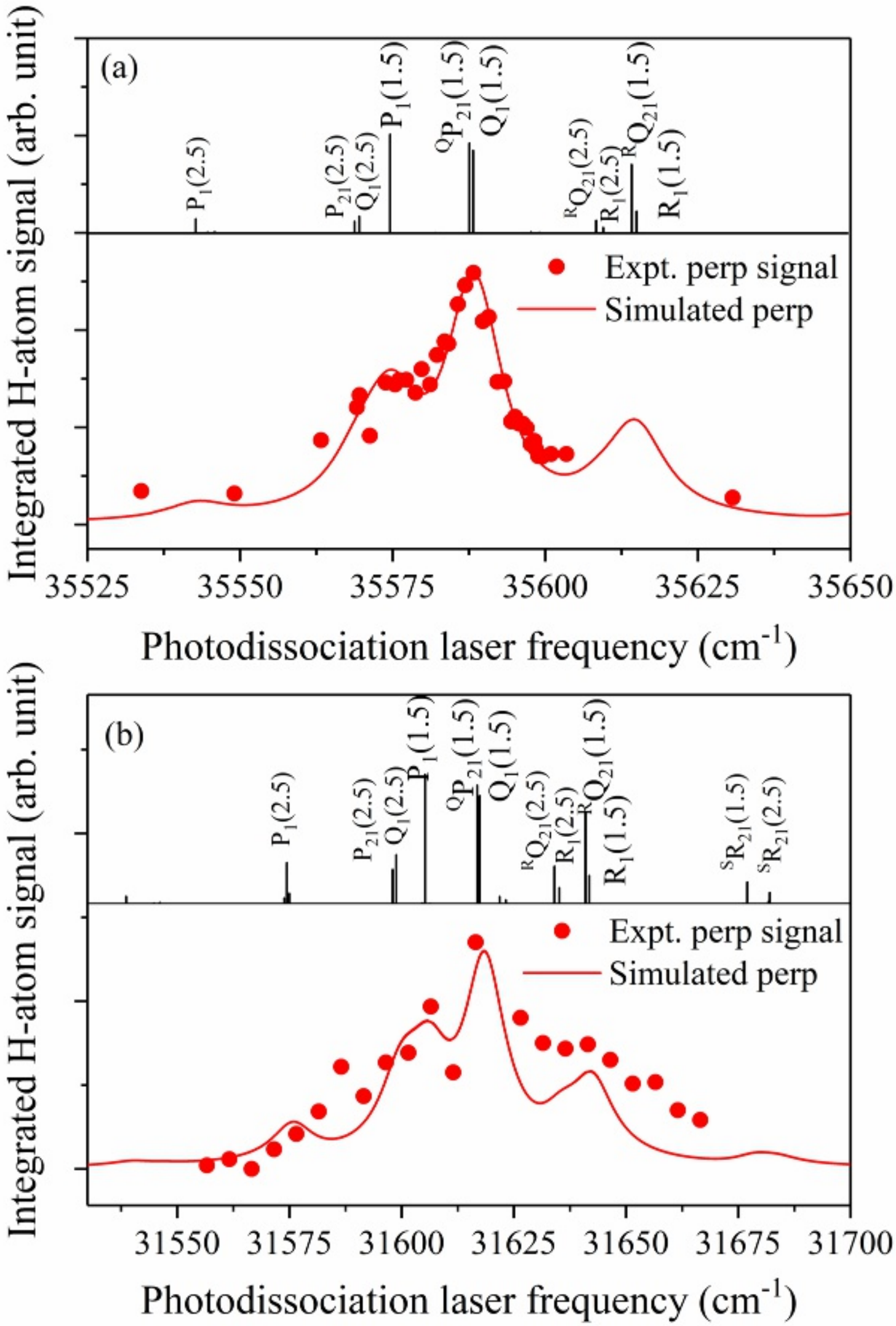
(a)
$P_1(2.5)$
$P_{21}(2.5)$
$Q_1(2.5)$
$P_1(1.5)$
$^{Q}P_{21}(1.5)$
$Q_1(1.5)$
$^{R}Q_{21}(2.5)$
$^{R}R_1(2.5)$
$^{R}Q_{21}(1.5)$
$R_1(1.5)$
Expt. perp signal
Simulated perp
Integrated H-atom signal (arb. unit)
35525
35550
35575
35600
35625
35650
Photodissociation laser frequency (cm^{-1})
(b)
$P_1(2.5)$
$P_{21}(2.5)$
$Q_1(2.5)$
$P_1(1.5)$
$^{Q}P_{21}(1.5)$
$Q_1(1.5)$
$^{R}Q_{21}(2.5)$
$^{R}R_1(2.5)$
$^{R}Q_{21}(1.5)$
$R_1(1.5)$
$^{S}R_{21}(1.5)$
$^{S}R_{21}(2.5)$
Expt. perp signal
Simulated perp
Integrated H-atom signal (arb. unit)
31550
31575
31600
31625
31650
31675
31700
Photodissociation laser frequency (cm^{-1})

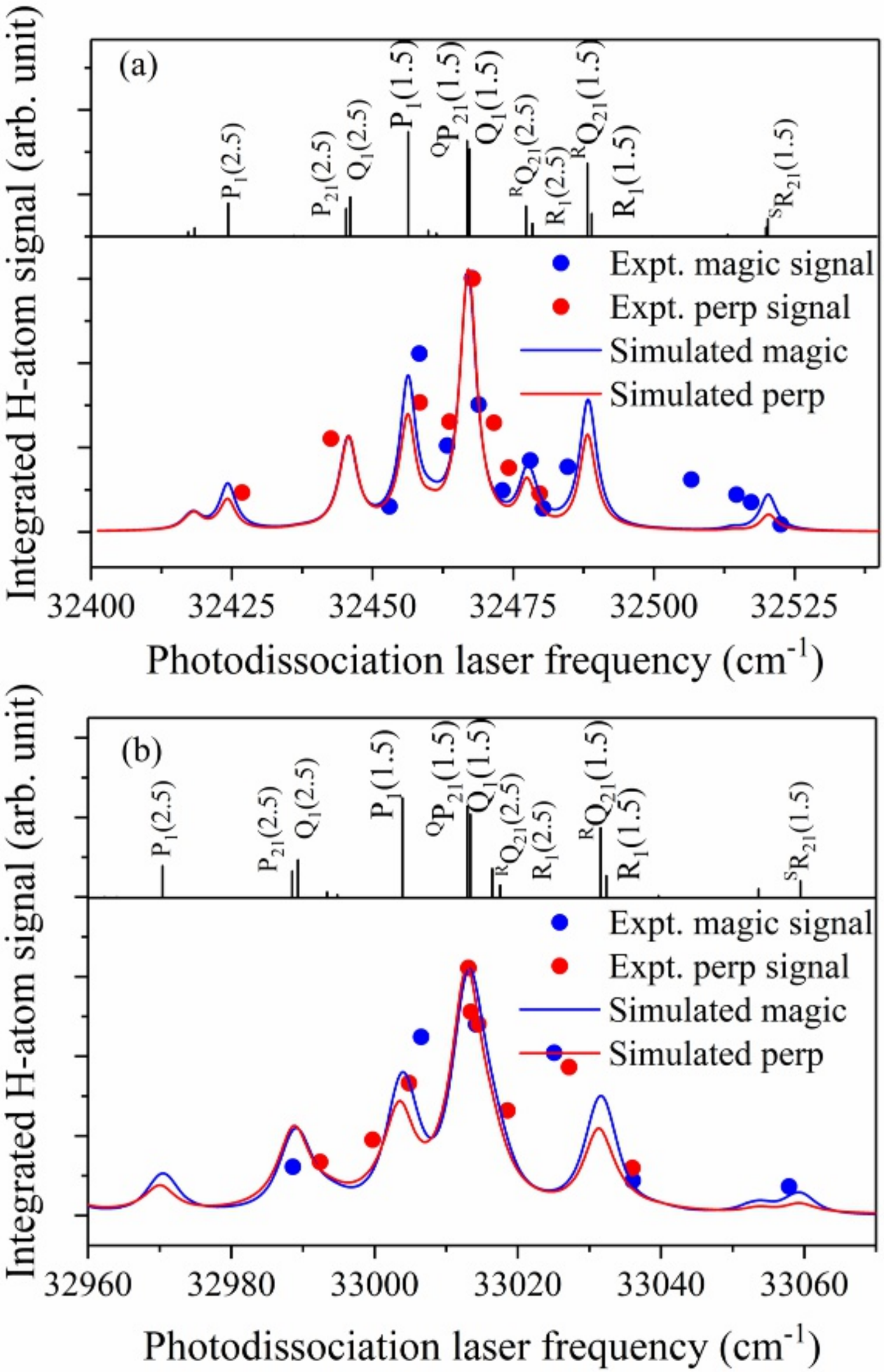
(a)
$P_1(2.5)$
$P_{21}(2.5)$
$Q_1(2.5)$
$P_1(1.5)$
$^{Q}P_{21}(1.5)$
$Q_1(1.5)$
$^{R}Q_{21}(2.5)$
$R_1(2.5)$
$^{R}Q_{21}(1.5)$
$R_1(1.5)$
$^{S}R_{21}(1.5)$
Expt. magic signal
Expt. perp signal
Simulated magic
Simulated perp
Integrated H-atom signal (arb. unit)
32400
32425
32450
32475
32500
32525
Photodissociation laser frequency (cm^{-1})
(b)
$P_1(2.5)$
$P_{21}(2.5)$
$Q_1(2.5)$
$P_1(1.5)$
$^{Q}P_{21}(1.5)$
$Q_1(1.5)$
$^{R}Q_{21}(2.5)$
$R_1(2.5)$
$^{R}Q_{21}(1.5)$
$R_1(1.5)$
$^{S}R_{21}(1.5)$
Expt. magic signal
Expt. perp signal
Simulated magic
Simulated perp
Integrated H-atom signal (arb. unit)
32960
32980
33000
33020
33040
33060
Photodissociation laser frequency (cm^{-1})

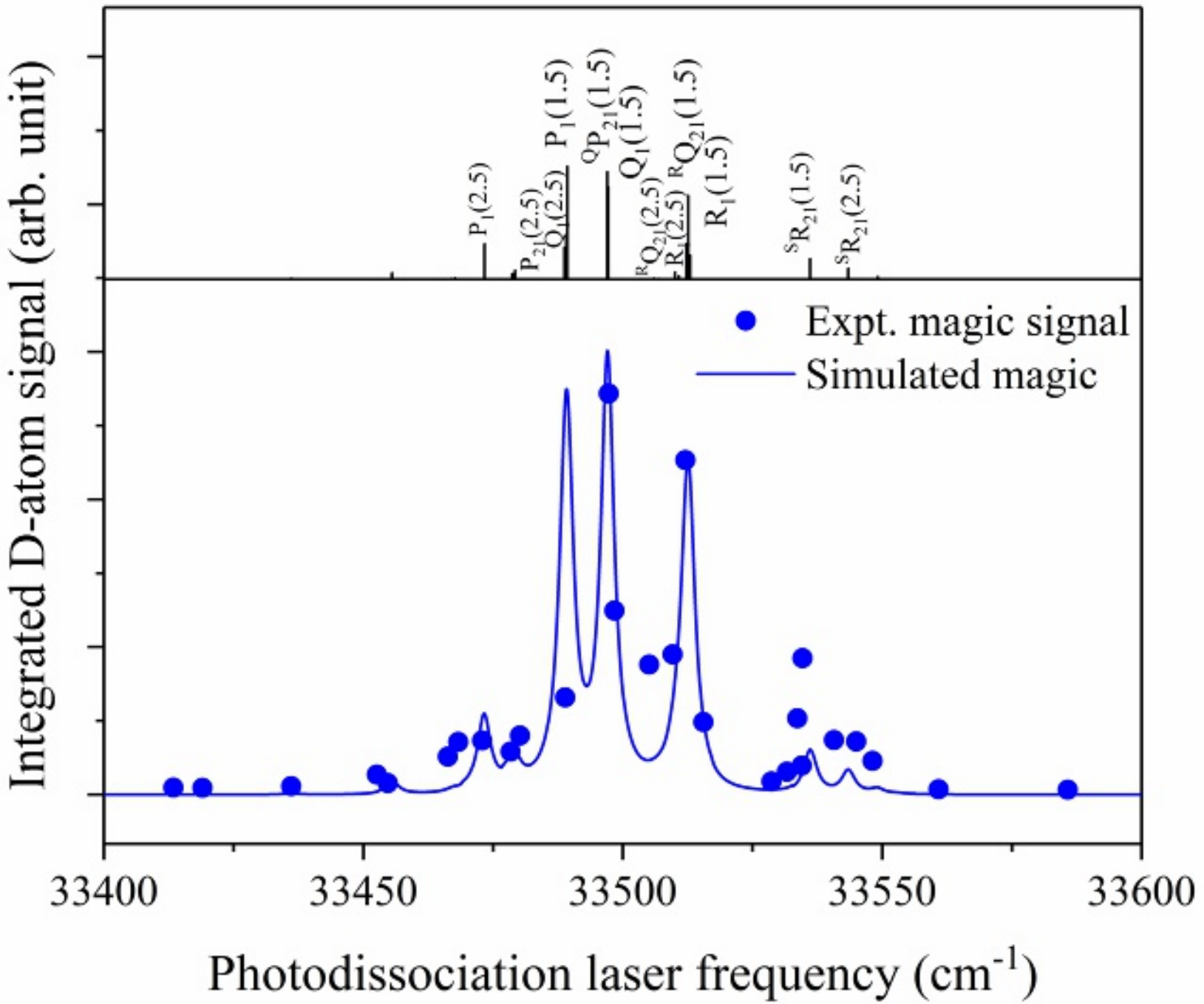
Integrated D-atom signal (arb. unit)
P1(2.5)
P21(2.5)
Q1(2.5)
P1(1.5)
OP21(1.5)
Q1(1.5)
RQ21(2.5)
RR1(2.5)
RQ21(1.5)
R1(1.5)
SR21(1.5)
SR21(2.5)
Expt. magic signal
Simulated magic
33400
33450
33500
33550
33600
Photodissociation laser frequency (cm-1)

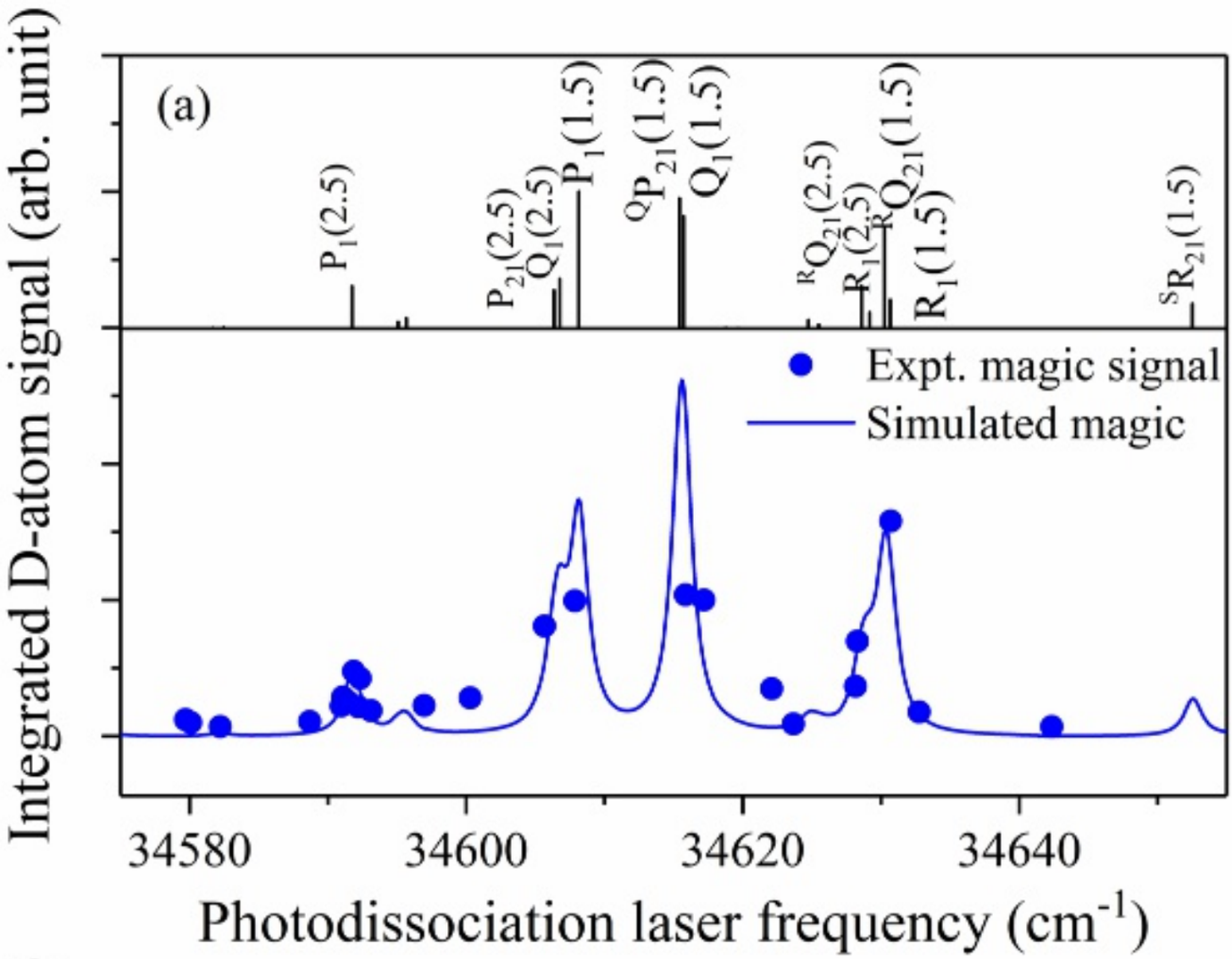
(a)
$P_1(2.5)$
$P_{21}(2.5)$
$Q_1(2.5)$
$P_1(1.5)$
$^{Q}P_{21}(1.5)$
$Q_1(1.5)$
$^{R}Q_{21}(2.5)$
$R_1(2.5)$
$^{R}Q_{21}(1.5)$
$R_1(1.5)$
$^{S}R_{21}(1.5)$
Expt. magic signal
Simulated magic
Integrated D-atom signal (arb. unit)
34580
34600
34620
34640
Photodissociation laser frequency (cm^{-1})

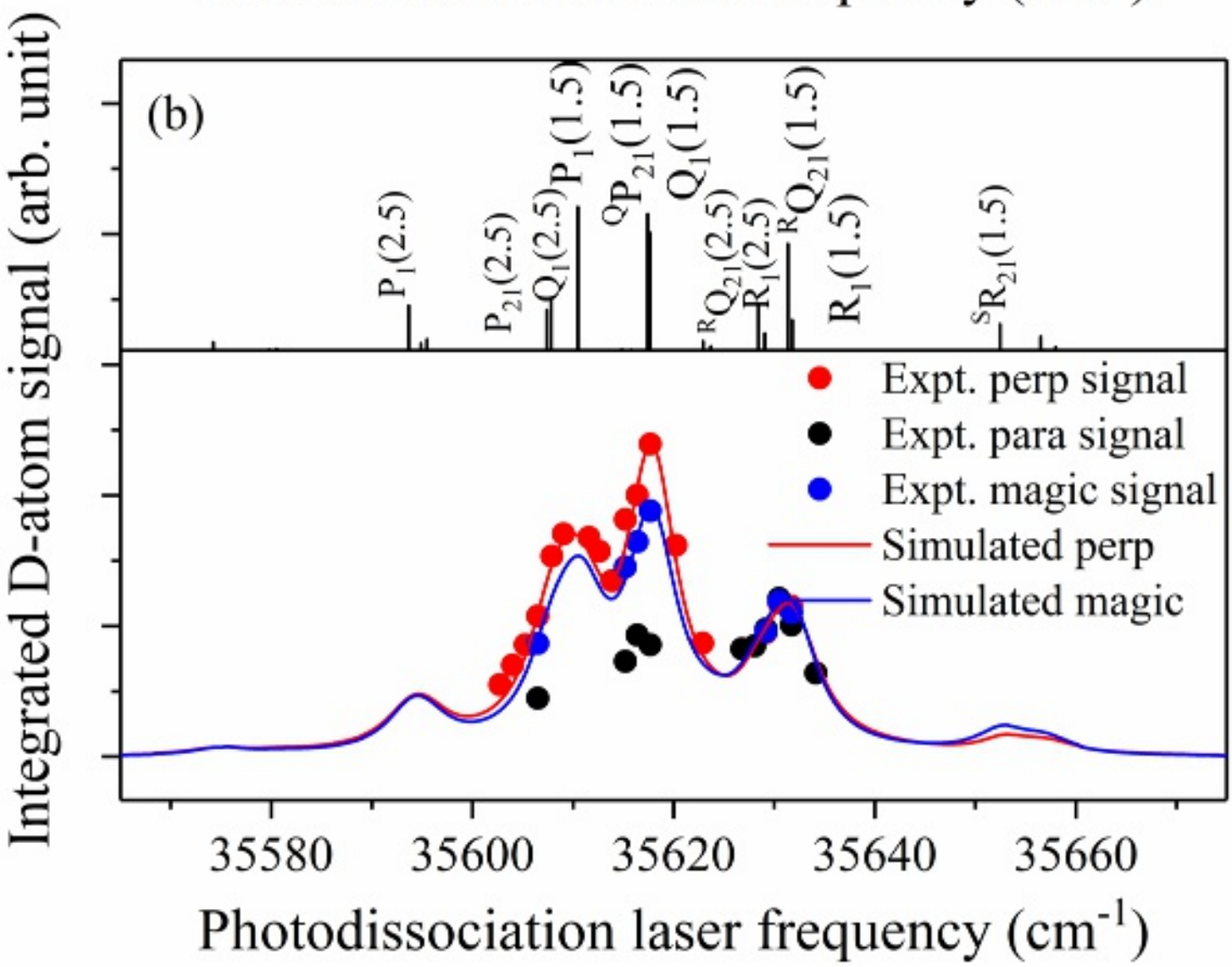
(b)
$P_1(2.5)$
$P_{21}(2.5)$
$Q_1(2.5)$
$P_1(1.5)$
$^{Q}P_{21}(1.5)$
$Q_1(1.5)$
$^{R}Q_{21}(2.5)$
$R_1(2.5)$
$^{R}Q_{21}(1.5)$
$R_1(1.5)$
$^{S}R_{21}(1.5)$
Expt. perp signal
Expt. para signal
Expt. magic signal
Simulated perp
Simulated magic
Integrated D-atom signal (arb. unit)
35580
35600
35620
35640
35660
Photodissociation laser frequency (cm^{-1})

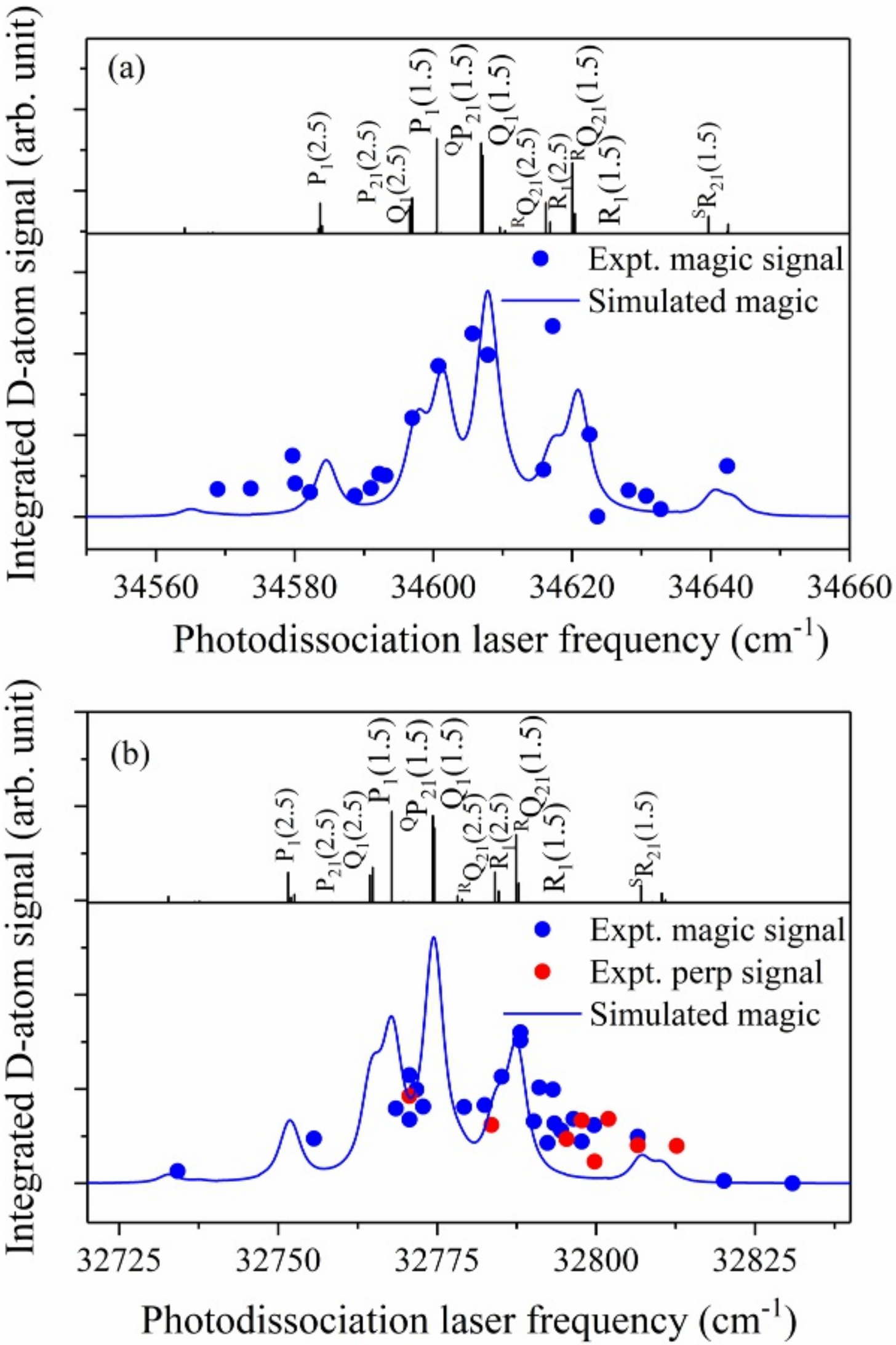
(a)
P1(2.5)
P21(2.5)
Q1(2.5)
P1(1.5)
QP21(1.5)
Q1(1.5)
RQ21(2.5)
R1(2.5)
RQ21(1.5)
R1(1.5)
SR21(1.5)
Expt. magic signal
Simulated magic
Integrated D-atom signal (arb. unit)
34560
34580
34600
34620
34640
34660
Photodissociation laser frequency (cm-1)
(b)
P1(2.5)
P21(2.5)
Q1(2.5)
P1(1.5)
QP21(1.5)
Q1(1.5)
RQ21(2.5)
R1(2.5)
RQ21(1.5)
R1(1.5)
SR21(1.5)
Expt. magic signal
Expt. perp signal
Simulated magic
Integrated D-atom signal (arb. unit)
32725
32750
32775
32800
32825
Photodissociation laser frequency (cm-1)

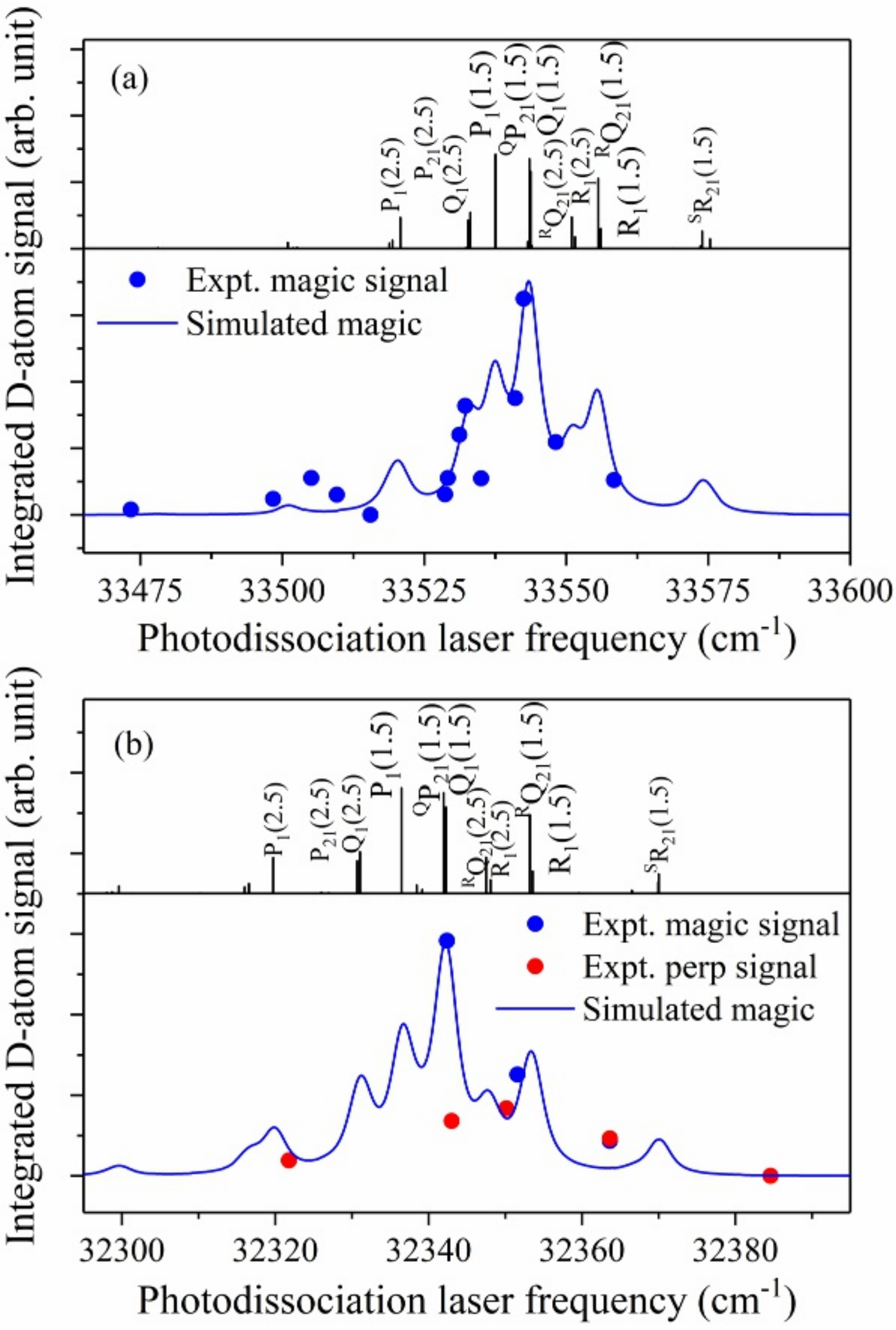
(a)
$P_1(2.5)$
$P_{21}(2.5)$
$Q_1(2.5)$
$P_1(1.5)$
$^{Q}P_{21}(1.5)$
$Q_1(1.5)$
$^{R}Q_{21}(2.5)$
$R_1(2.5)$
$^{R}Q_{21}(1.5)$
$R_1(1.5)$
$^{S}R_{21}(1.5)$
Expt. magic signal
Simulated magic
Integrated D-atom signal (arb. unit)
33475
33500
33525
33550
33575
33600
Photodissociation laser frequency (cm^{-1})
(b)
$P_1(2.5)$
$P_{21}(2.5)$
$Q_1(2.5)$
$P_1(1.5)$
$^{Q}P_{21}(1.5)$
$Q_1(1.5)$
$^{R}Q_{21}(2.5)$
$R_1(2.5)$
$^{R}Q_{21}(1.5)$
$R_1(1.5)$
$^{S}R_{21}(1.5)$
Expt. magic signal
Expt. perp signal
Simulated magic
Integrated D-atom signal (arb. unit)
32300
32320
32340
32360
32380
Photodissociation laser frequency (cm^{-1})

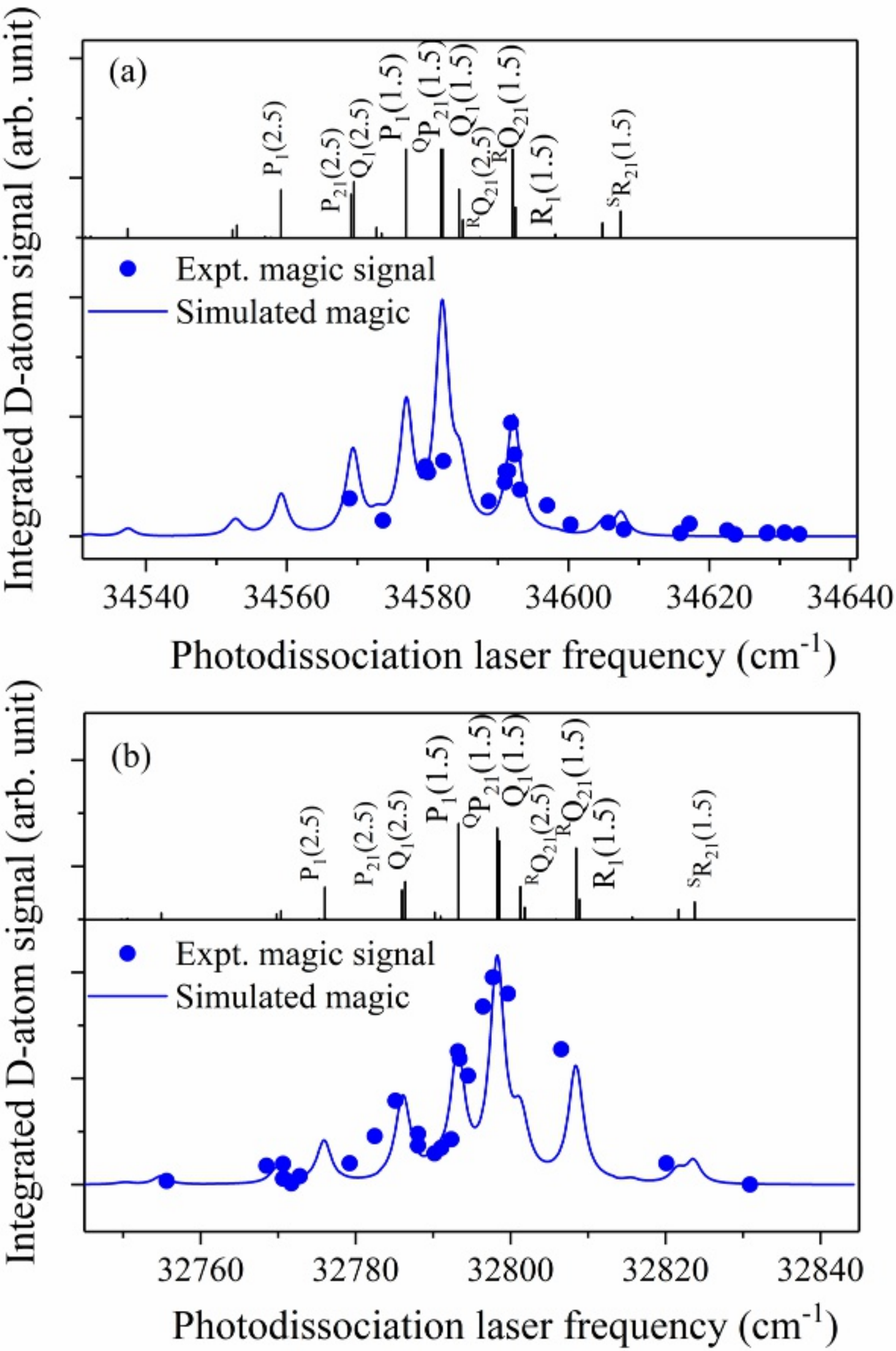
(a)
$P_1(2.5)$
$P_{21}(2.5)$
$Q_1(2.5)$
$P_1(1.5)$
$^{Q}P_{21}(1.5)$
$Q_1(1.5)$
$^{R}Q_{21}(2.5)$
$^{R}Q_{21}(1.5)$
$R_1(1.5)$
$^{S}R_{21}(1.5)$
Expt. magic signal
Simulated magic
Integrated D-atom signal (arb. unit)
34540
34560
34580
34600
34620
34640
Photodissociation laser frequency (cm^{-1})
(b)
$P_1(2.5)$
$P_{21}(2.5)$
$Q_1(2.5)$
$P_1(1.5)$
$^{Q}P_{21}(1.5)$
$Q_1(1.5)$
$^{R}Q_{21}(2.5)$
$^{R}Q_{21}(1.5)$
$R_1(1.5)$
$^{S}R_{21}(1.5)$
Expt. magic signal
Simulated magic
Integrated D-atom signal (arb. unit)
32760
32780
32800
32820
32840
Photodissociation laser frequency (cm^{-1})

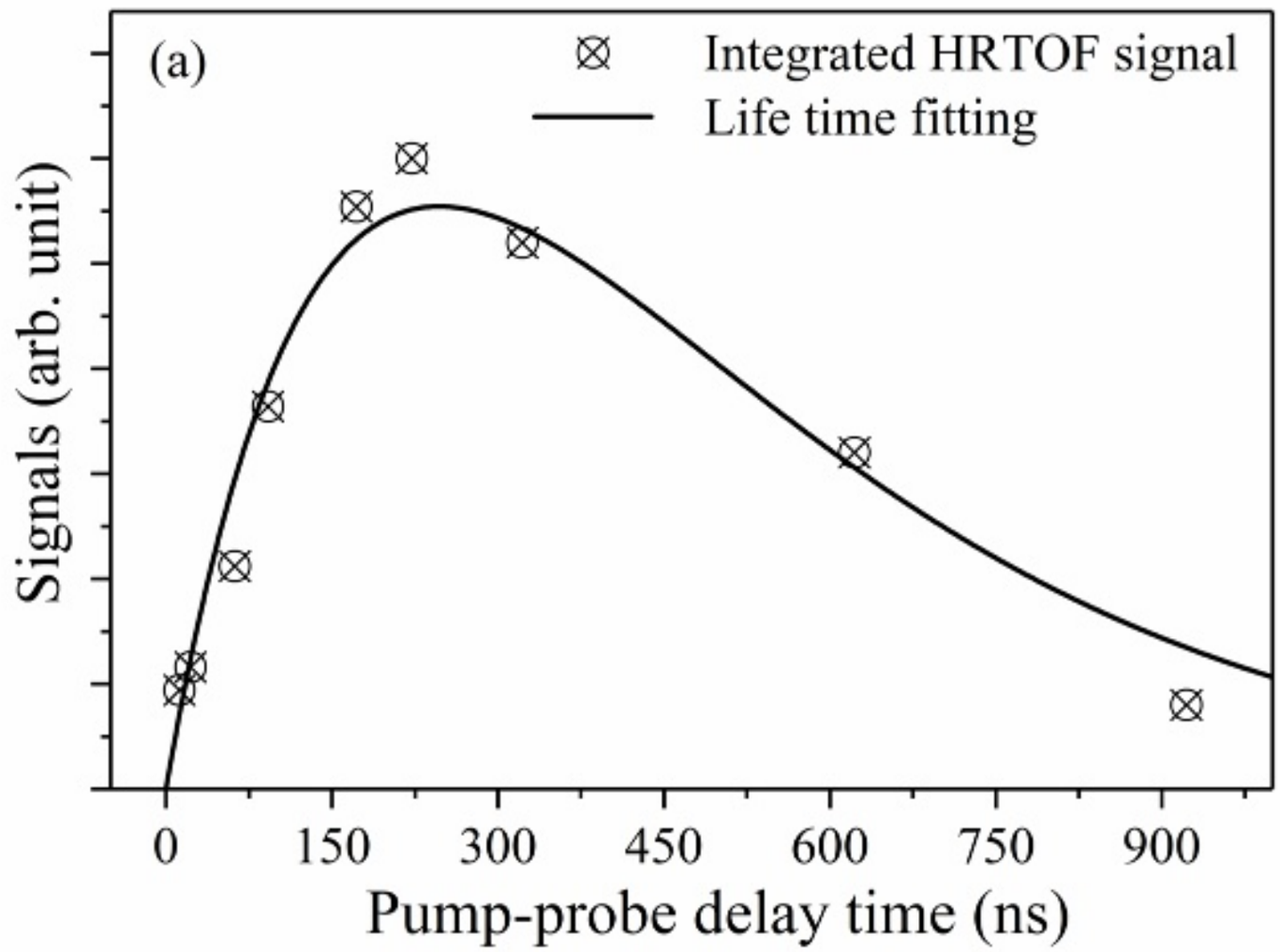
(a)
Integrated HRTOF signal
Life time fitting
Signals (arb. unit)
0
150
300
450
600
750
900
Pump-probe delay time (ns)

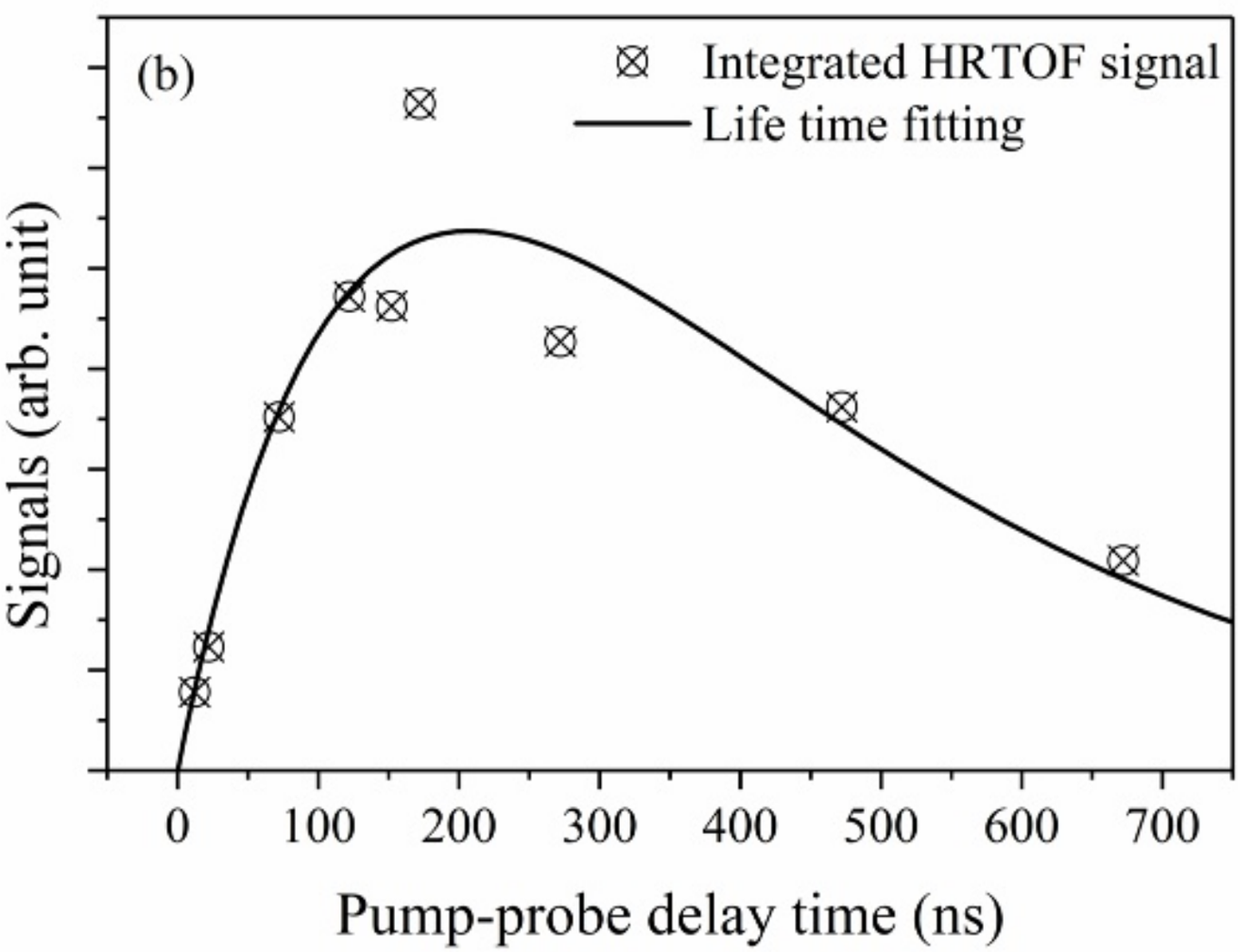
(b)
Integrated HRTOF signal
Life time fitting
Signals (arb. unit)
0
100
200
300
400
500
600
700
Pump-probe delay time (ns)